AD-A031 332 PRINCETON UNIV N J DEPT OF ELECTRICAL ENGINEERING F/G 20/12
STUDY OF ELECTRONIC TRANSPORT AND TRAPPING IN TECHNOLOGICALLY I--ETC(U
APR 76 W C JOHNSON N00014-75-C-1074

UNCLASSIFIED NL

1 OF 1
ADA031332

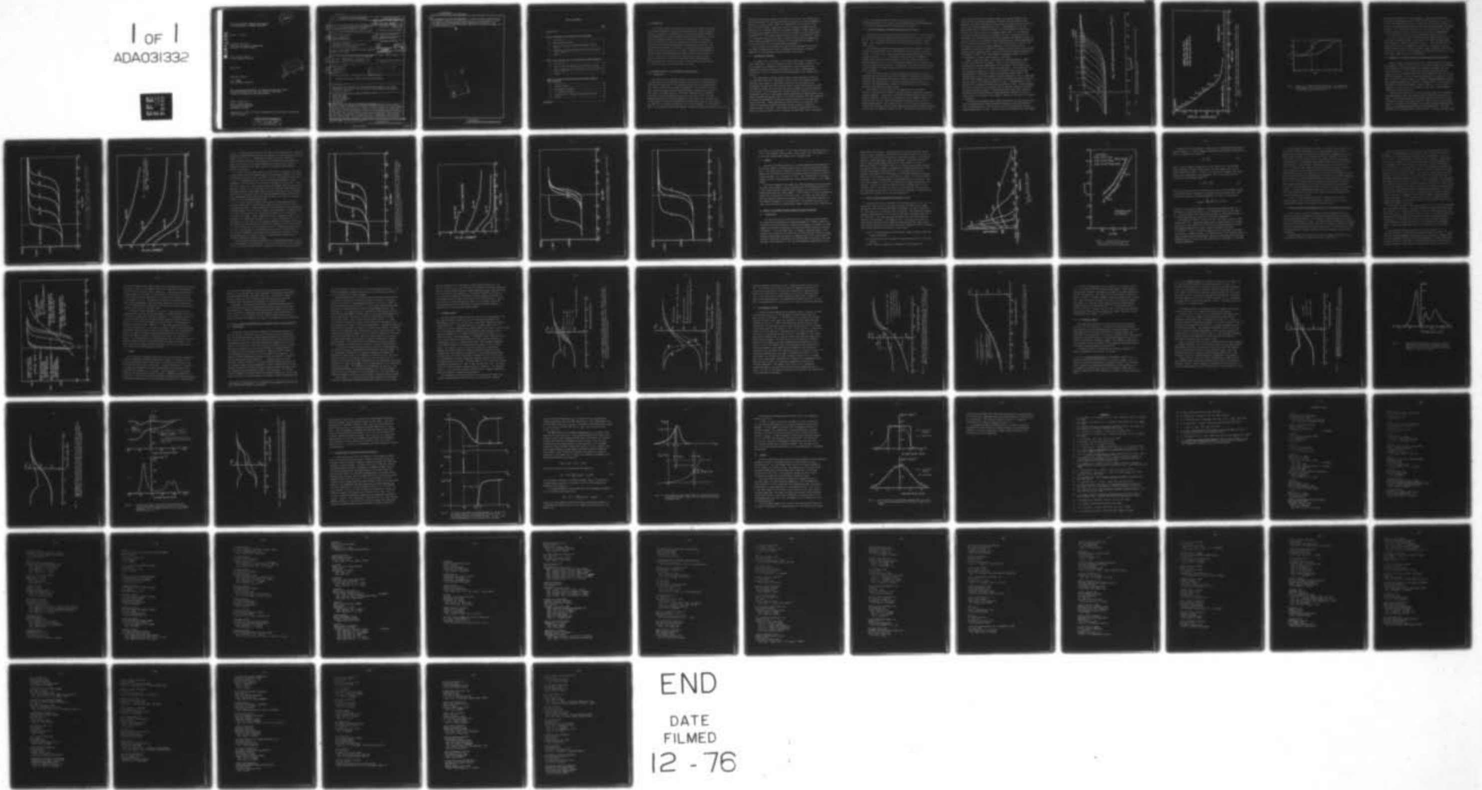

END
DATE
FILMED
12 - 76

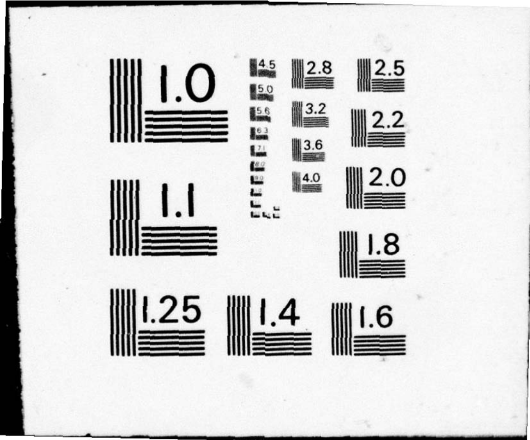
1.0
4.5
5.0
5.6
2.8
3.2
3.6
4.0
2.5
2.2
2.0
1.1
1.8
1.25
1.4
1.6

(12)

STUDY OF ELECTRONIC TRANSPORT AND TRAPPING IN TECHNOLOGICALLY IMPORTANT INSULATORS

AD A031332

Walter C. Johnson

Princeton University
Department of Electrical Engineering
Princeton, New Jersey 08540

Final Technical Report
Contract N00014-75-C-1074

D D C
RECEIVED
OCT 28 1976
C

April 1976

Scientific Officer:

H. L. Hughes
Naval Research Laboratory

This research was sponsored by the Defense Nuclear Agency under Subtask Z99QAXTA007, Work Unit 52, Work Title "Electronic Transport and Trapping in Thin Film Oxides."

Report Prepared for:

Office of Naval Research
Naval Research Laboratory
Washington, DC 20390

Reproduction in whole or in part is permitted for any purpose of the United States Government.

DISTRIBUTION STATEMENT A
Approved for public release;
Distribution Unlimited

Unclassified

SECURITY CLASSIFICATION OF THIS PAGE (When Data Entered)

REPORT DOCUMENTATION PAGE		READ INSTRUCTIONS BEFORE COMPLETING FORM
1. REPORT NUMBER	2. GOVT ACCESSION NO.	3. RECIPIENT'S CATALOG NUMBER (9) Final Rept.
4. TITLE (6) STUDY OF ELECTRONIC TRANSPORT AND TRAPPING IN TECHNOLOGICALLY IMPORTANT INSULATORS.		5. TYPE OF REPORT & PERIOD COVERED Scientific - Final
		6. PERFORMING ORG. REPORT NUMBER
7. AUTHOR(s) (10) Walter C./Johnson		8. CONTRACT OR GRANT NUMBER(s) (15) N00014-75-C-1074 NEW
9. PERFORMING ORGANIZATION NAME AND ADDRESS Princeton University Department of Electrical Engineering Princeton, New Jersey 08540		10. PROGRAM ELEMENT, PROJECT, TASK AREA & WORK UNIT NUMBERS (11) (12) 52p.
11. CONTROLLING OFFICE NAME AND ADDRESS Office of Naval Research/Naval Research Laboratory Washington, DC 20390		12. REPORT DATE April 1976
		13. NUMBER OF PAGES 72
14. MONITORING AGENCY NAME & ADDRESS (if different from Controlling Office) (16) DNA-NWED-QAXT		15. SECURITY CLASS. (of this report)
		15a. DECLASSIFICATION/DOWNGRADING SCHEDULE

16. DISTRIBUTION STATEMENT (of this Report)

(17) A007

DISTRIBUTION STATEMENT A
Approved for public release;
Distribution Unlimited

17. DISTRIBUTION STATEMENT (of the abstract entered in Block 20, if different from Report)

Approved for public release; distribution unlimited

18. SUPPLEMENTARY NOTES

This research was sponsored by the Defense Nuclear Agency under Subtask Z99QAXTA007, Work Unit 52, Work Title "Electronic Transport and Trapping in Thin Film Oxides."

19. KEY WORDS (Continue on reverse side if necessary and identify by block number)

Insulating Films
Radiation Damage
Radiation Hardening
Silicon Dioxide
MOS Devices

20. ABSTRACT (Continue on reverse side if necessary and identify by block number)

Studies of electron trapping in unannealed aluminum-implanted silicon-dioxide films show large concentrations of electron traps not present in control samples. A substantial fraction of the traps appear to be associated with displacement damage created by the implantation. A study of electron-beam-induced conduction in thermally grown silicon dioxide indicates that substantial concentrations of electron traps are generated through the oxide by bombardment with a nonpenetrating electron beam. This conclusion has been confirmed by investigation of the electron-trapping properties of oxides that had previously been subjected

DD FORM 1 JAN 73 1473 EDITION OF 1 NOV 65 IS OBSOLETE
S/N 0102-014-6601

Unclassified

SECURITY CLASSIFICATION OF THIS PAGE (When Data Entered)

400734

1/B

20.

to nonpenetrating electron bombardment. A study of lateral nonuniformities and interface states in MIS structures has led to the development of three new methods for distinguishing between these two effects and to a new and simple method for determining the distribution of flatband voltages in a nonuniform MIS capacitor.

ACCESSION for
NTIS White Section
DDC B.ff Section
UNANNOUNCED
JUSTIFICATION
BY
DISTRIBUTION/AVAILABILITY CODES
Dist. AVAIL. and/or SPECIAL
A

TABLE OF CONTENTS

Page

1. Introduction 1

2. Electron Trapping in Ion-Implanted Silicon Dioxide

2.1. Introduction 1

2.2. Experimental Procedure 2

2.3. Electron Trapping in Aluminum-Implanted Silicon Dioxide 3

2.4. Comparison of Aluminum-Implanted and Neon-Implanted Silicon Dioxide 8

2.5. Summary 16

3. Effects of Low-Energy Electron Irradiation on MOS Capacitors

3.1. Introduction 16

3.2. Study of Electron-Beam-Induced Conduction in SiO_2 .. 17

3.3. Study of Electron Traps Generated in SiO_2 by Electron-Beam Irradiation 21

3.4. Summary 24

4. Study of Lateral Nonuniformities and Interface States in MIS Structures

4.1. Introduction 25

4.2. Frequency Method 27

4.3. Low-Temperature Method 30

4.4. C-V Comparison Method 33

4.5. Determination of Flatband Voltage Distribution 40

4.6. Summary 44

REFERENCES 47

1. INTRODUCTION

This report presents the results of three sets of studies concerning the radiation hardness of metal-insulator-semiconductor (MIS) structures. Section 2 describes an investigation of the electron-trapping properties of aluminum-implanted and neon-implanted silicon-dioxide films on silicon. Section 3 gives the results of a study of the effects of low-energy electron irradiation on thermally grown silicon dioxide and shows that such irradiation generates substantial concentrations of electron traps in the oxide well ahead of the range of the primary electrons themselves. Section 4 describes the results of a study of methods for distinguishing between lateral nonuniformities and interface states in MIS structures and for characterizing nonuniformities when they are found to exist. Three new methods are proposed for detecting lateral nonuniformities, and a new and simple method is proposed for determining the distribution of flatband voltages in a nonuniform MIS structure.

2. ELECTRON TRAPPING IN ION-IMPLANTED SILICON DIOXIDE

2.1. Introduction

The implantation of impurity ions into the SiO_2 layer of an MOS device has been shown to reduce the sensitivity of the device to ionizing radiation under positive gate bias.[1-5] The radiation sensitivity of thermally grown SiO_2 films on silicon was proposed by Zaininger[6] to be the result of strong hole trapping and weak electron trapping following generation of electron-hole pairs by ionizing radiation. Williams[7] demonstrated that thermally grown SiO_2 films are relatively free of electron traps ($\sim 10^{14}$ cm^{-3}) and Goodman[8] found that the electron mobility is relatively high (~ 30 cm^2/V sec). The experiments of Powell and Derbenwick[9] indicate that holes can drift through the oxide but are strongly trapped near the $Si\text{-}SiO_2$ interface. The following model of the radiation effect thus emerges. When an MOS device is exposed to ionizing

radiation, electron-hole pairs are generated in the oxide. For positive gate bias the electrons drift through the oxide to the gate, with some recombination probably occurring en route. Holes are transported to the vicinity of the Si-SiO_2 interface where a significant fraction of them are trapped, thereby giving rise to a negative shift in the flatband voltage of an MOS capacitor, or equivalently to a negative shift in the turn-on voltage of an MOS field-effect transistor.[10,11] This model suggests that the reduction in sensitivity caused by ion implantation may be the result of electron traps and/or recombination centers which are generated in the SiO_2 by the implantation and which act to reduce the buildup of a net charge during irradiation.

Here we present the results of a study in which photoelectric and MOS capacitance techniques were used to investigate deep electron trapping in aluminum- and neon-implanted thermally grown silicon dioxide.

2.2. Experimental Procedure

Our samples were fabricated on 1-5 ohm-cm n-type silicon wafers with (100) orientation. The oxide films were grown in dry oxygen at 1000°C. Some of the samples were implanted with aluminum ions, others with neon ions. Unimplanted control sections were provided in all cases. Semitransparent field plates of gold or aluminum were vacuum-evaporated on the exposed oxide surface.

The experimental procedure that we used to study the electron traps in the oxide was as follows. The metallic field plate of the sample was biased positively with respect to the silicon substrate, and the structure was illuminated from the front with photons having an energy smaller than the oxide band gap but greater than the electronic barrier between the silicon substrate and the oxide. For this purpose we used photons with an energy of 4.8 eV. A substantial fraction of the incident photons penetrated the semitransparent field plate and passed through the oxide to the Si-SiO_2 interface where they stimulated an internal photoemission of electrons from the silicon into the conduction band of the oxide. These electrons were then drifted by the electric field toward the positively biased field plate and were subject to capture by electron traps in the oxide. The storage of negative charge resulting from electron capture produced a shift in flatband voltage which could be determined

from the high-frequency MOS capacitance-voltage (C-V) characteristic. Subsequent discharge of the traps could be accomplished by photodepopulation or by thermal annealing with the contacts short circuited.

2.3. Electron Trapping in Aluminum-Implanted Silicon Dioxide

This study was performed on dry-grown 1400Å SiO_2 films. The oxide of one section of the wafer was implanted with aluminum ions at 20 keV to a fluence of 10^{14} cm^{-2}. The other section was not implanted and served as a control sample. Semitransparent electrodes of gold were vacuum evaporated on the front surface.

The unannealed aluminum-implanted samples initially displaced flatband voltages of approximately -15 V, indicating an initial storage of positive charge. In contrast, the control samples showed only small initial flatband voltages, typically - 1 V. The positive space charge in the implanted samples was neutralized almost completely, and the flatband voltage was brought essentially to zero, by irradiating the sample with 4.8 eV photons with the contacts short circuited. Alternatively, the initial positive charge could be removed by thermal annealing at 450°C for 30 min with the contacts short circuited.

After the initial positive charge had been neutralized, the electron trapping properties of the oxide were investigated by biasing the field plate positively and illuminating the sample to produce an internal photoemission of electrons from the substrate. The sample current was monitored and, at intervals, the high-frequency (1 MHz) C-V characteristic of the sample was measured to determine the charge storage.

The injection of electrons into the unimplanted control samples resulted in essentially no change in flatband voltage, indicating negligible electron trapping. In contrast, the aluminum-implanted samples showed strong electron trapping. Typical results obtained on an Al-implanted sample are shown in Figs. 1 and 2. Here the field-plate voltage was held at + 10 V during photoinjection. As is shown in Fig. 1, the C-V curves shifted to the right as the photoinjection proceeded, indicating a buildup of negative charge in the oxide. An important feature in Fig. 1 is that the steady-state value

of the flat-band voltage is virtually equal to the voltage applied to the field plate during the photoinjection, indicating that the negative space charge of the trapped electrons was great enough to bring the electric field at the Si-SiO_2 interface approximately to zero. Corresponding to this, the photocurrent fell to a small value which could be attributed to stray photoemission from other surfaces in the sample chamber (Fig. 2). An analysis, the details of which are given in References 12 and 13, indicated that (1) essentially all injected electrons had been trapped in the implanted oxide, (2) that the centroid of the negative charge distribution was located approximately 670 Å from the field plate, and (3) that the observed decay in current could be explained by the electric-field dependence of the photoinjection as determined by Berglund and Powell.[14] The negative space charge in the implanted samples could be annealed either optically by photons of energy exceeding 4 eV or thermally at 350°C. The traps themselves remained, however, and could be recharged by a further photoinjection of electrons.

Figure 3 shows the effect of annealing the aluminum-implanted sample at 600°C for 30 min in dry nitrogen. Curve A is the high-frequency C-V relationship as measured immediately after the anneal. Curve B shows the effect on the C-V curve of an internal photoinjection of electrons for 25 min with a sample voltage of 10 V. This is a saturated curve; an additional photoinjection of electrons produced no appreciable further effect. The rightward shift of Curve B is smaller than that observed in Fig. 1, indicating that electron trapping has been reduced below the amount which would bring the electric field at the injecting interface to zero. Correspondingly, it was observed that a steady-state photocurrent continued to flow. The posttrapping C-V curve is stretched out in a manner such as would be caused by a laterally nonuniform storage of charge.[15] Further experiments along these lines were discontinued when difficulties were experienced with adhesion of the gold field plates to the surface of the samples. However, we can draw the following conclusions:

The 1400-Å Al-implanted sample trapped essentially all injected electrons, and the resulting space charge brought the injected current approximately to zero, indicating that the electric field at the Si-SiO_2 interface had been reduced approximately to zero. Similar results were obtained up to the highest

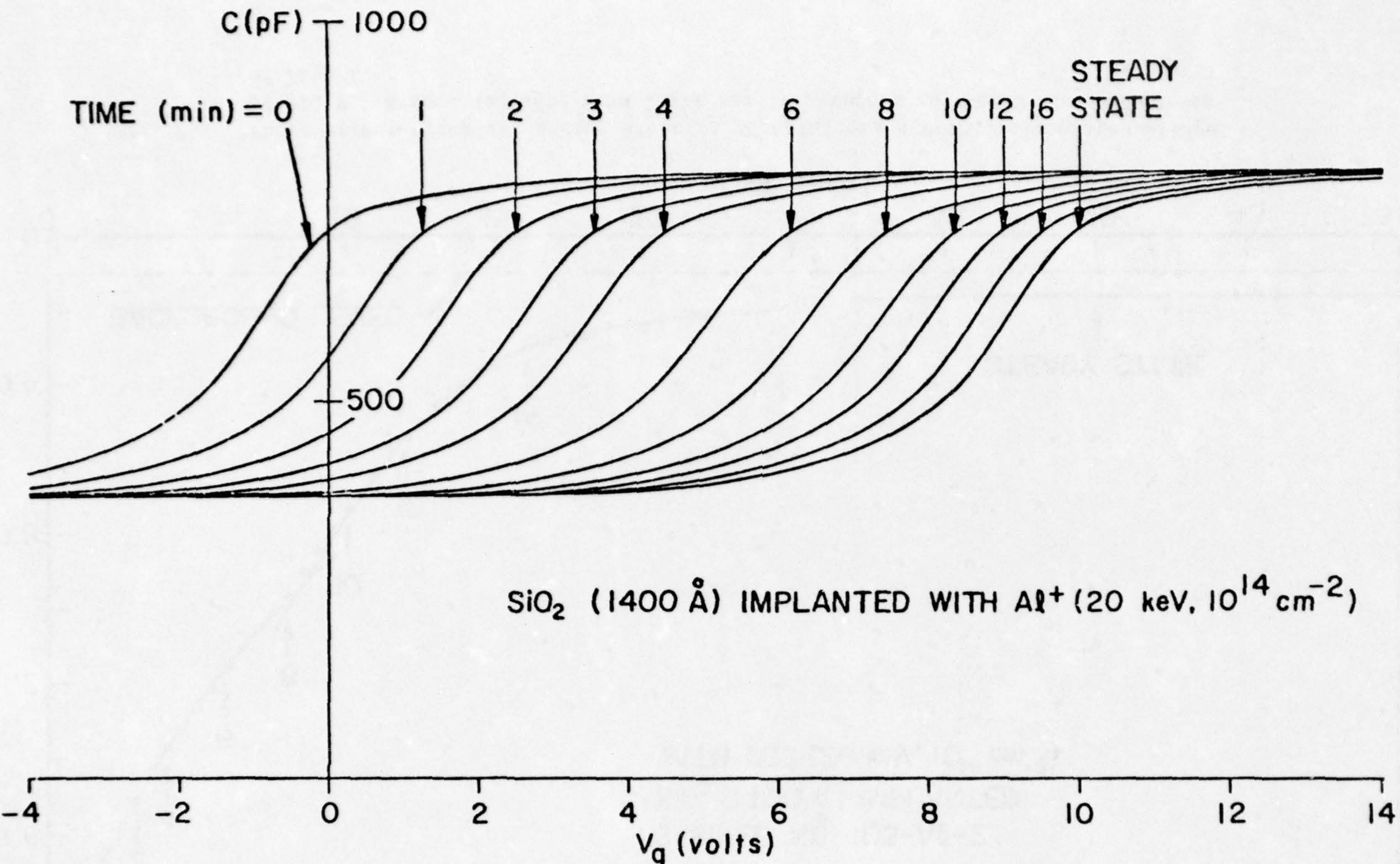

Fig. 1. Voltage shifts of the C-V curve with time during electron photoinjection with a field-plate voltage of +10 V.

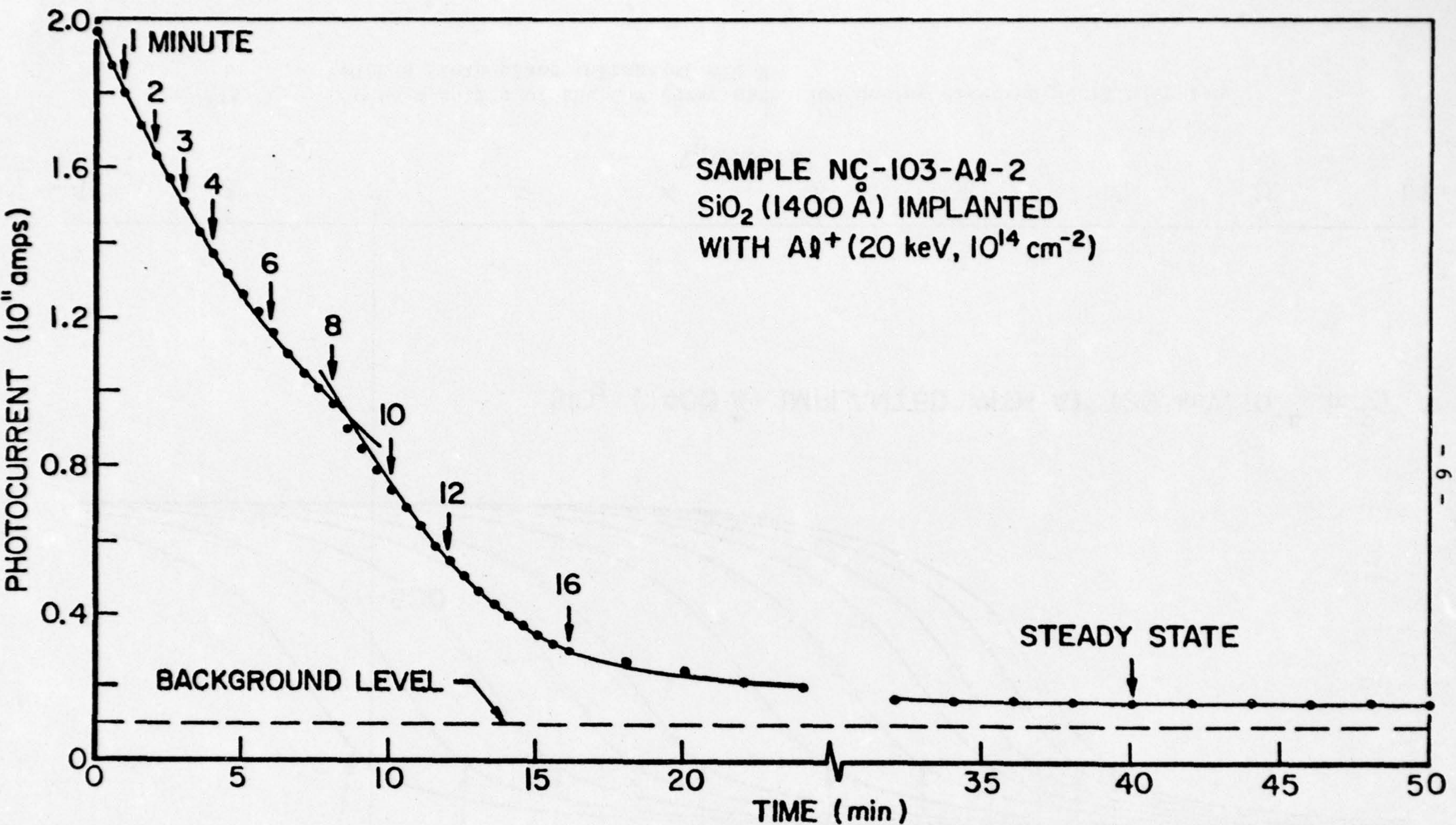

Fig. 2. Photocurrent transient during electron photoinjection with field-plate voltage of +10 V. Arrows indicate when light was interrupted to record the C-V curves of Fig. 1.

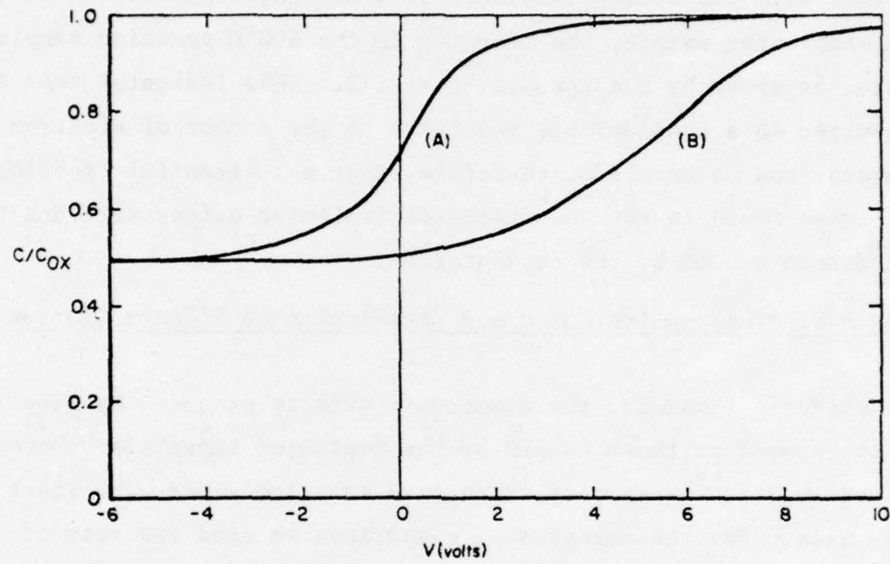

Fig. 3. Effect of an anneal at 600°C for 30 min. (A) Immediately after anneal. (B) After photoinjection of electrons for 25 min with sample voltage of 10 V.

field-plate voltages (35 V on these samples). With the centroid of the trapped charge approximately at the center of the oxide layer, i.e., near the front of the implantation profile, it seems clear that the total number of electron traps must have been much greater than the observed number of trapped electrons. At a field-plate voltage of 35 V, the concentration of trapped electrons required to bring the interface field to zero is approximately 5×10^{12} cm^{-2}, which is well below the implantation dose of 10^{14} cm^{-2}.

In contrast with the almost complete electron trapping observed in the unannealed Al-implanted sample, the trapping in the 600°C annealed sample was incomplete, as shown by the results of Fig. 3. This indicates that the annealing resulted in a considerable reduction in the number of electron trapping centers, and we conclude, therefore, that a substantial fraction of the electron traps found in the unannealed Al-implanted oxides were due to the displacement damage caused by the implantation.

2.4. Comparison of Aluminum-Implanted and Neon-Implanted Silicon Dioxide

Further evidence regarding the electronic effects produced by displacement damage as opposed to those caused by the implanted impurities themselves can be obtained by studying samples which have been implanted with inert atoms such as neon. For the purposes of comparison we used two sets of samples which were identical except that one was implanted with neon and the other with aluminum. The SiO_2 films had been grown in dry oxygen to a thickness of 1000 Å on 3 ohm-cm (100) n-Si substrates (sample designation HLH-01). The aluminum was implanted at 20 keV to a fluence of 10^{15} cm^{-2}. The neon was implanted at 20 keV to the somewhat greater fluence of 1.5×10^{15} cm^{-2} to compensate, to first order, for its smaller atomic mass. Semi-transparent aluminum field plates were used.

Figure 4 shows the effect of electron photoinjection into an unannealed aluminum-implanted oxide, using various gate voltages as indicated in the figure. At each gate voltage, electrons were photo-injected for 15-20 min to charge the traps and the high-frequency (1 MHz) C-V curve was then taken. Except at the highest gate voltages, the flat-band voltage was approximately equal to the gate voltage applied during the photoinjection. The time dependence of the photocurrents is shown in Fig. 5. For gate voltages greater

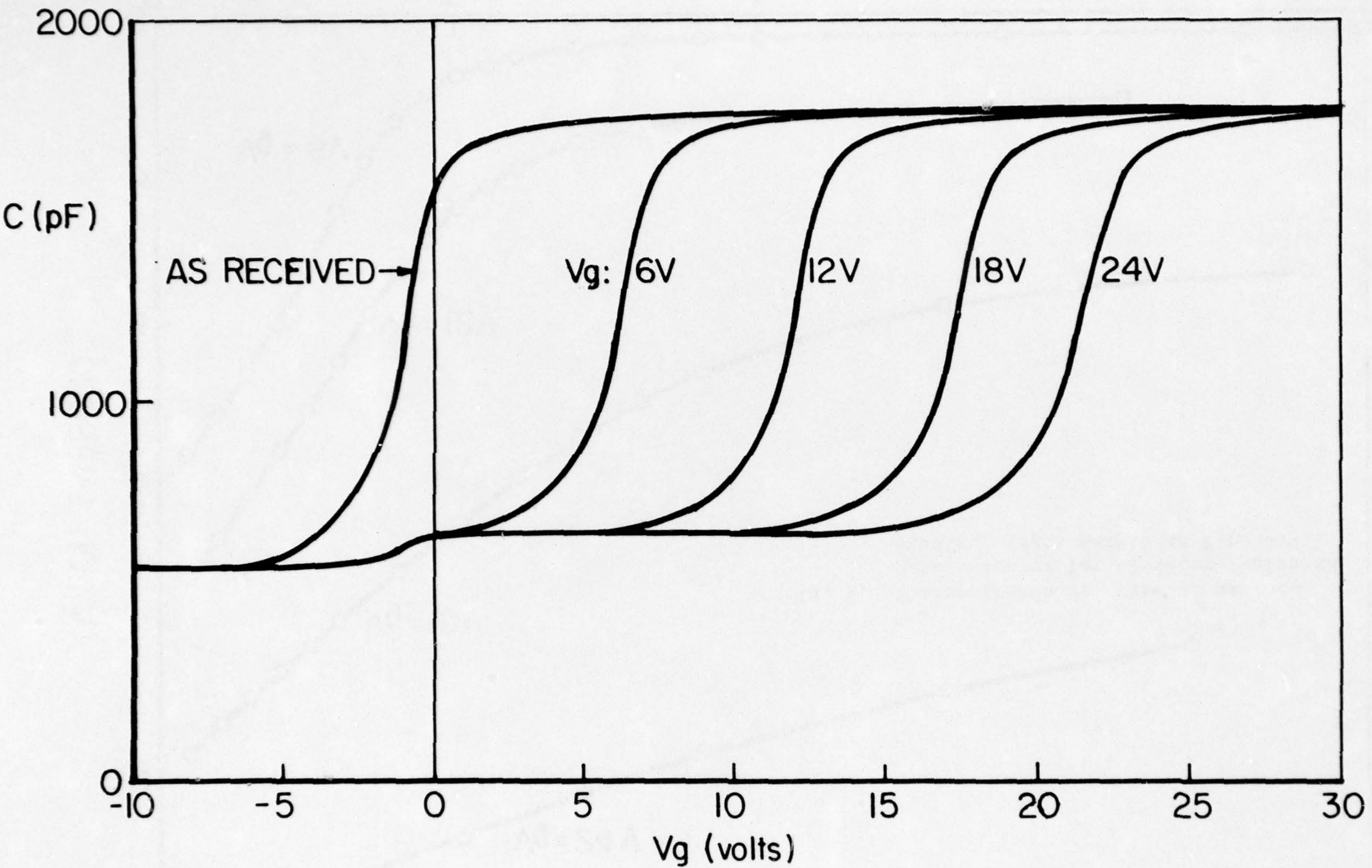

Fig. 4. Effect on the C-V curves of electron photoinjection at various field-plate voltages for aluminum-implanted sample. Silicon dioxide 1000 Å thick, implanted with Al at 20 keV to fluence of 10^{15} cm^{-2}.

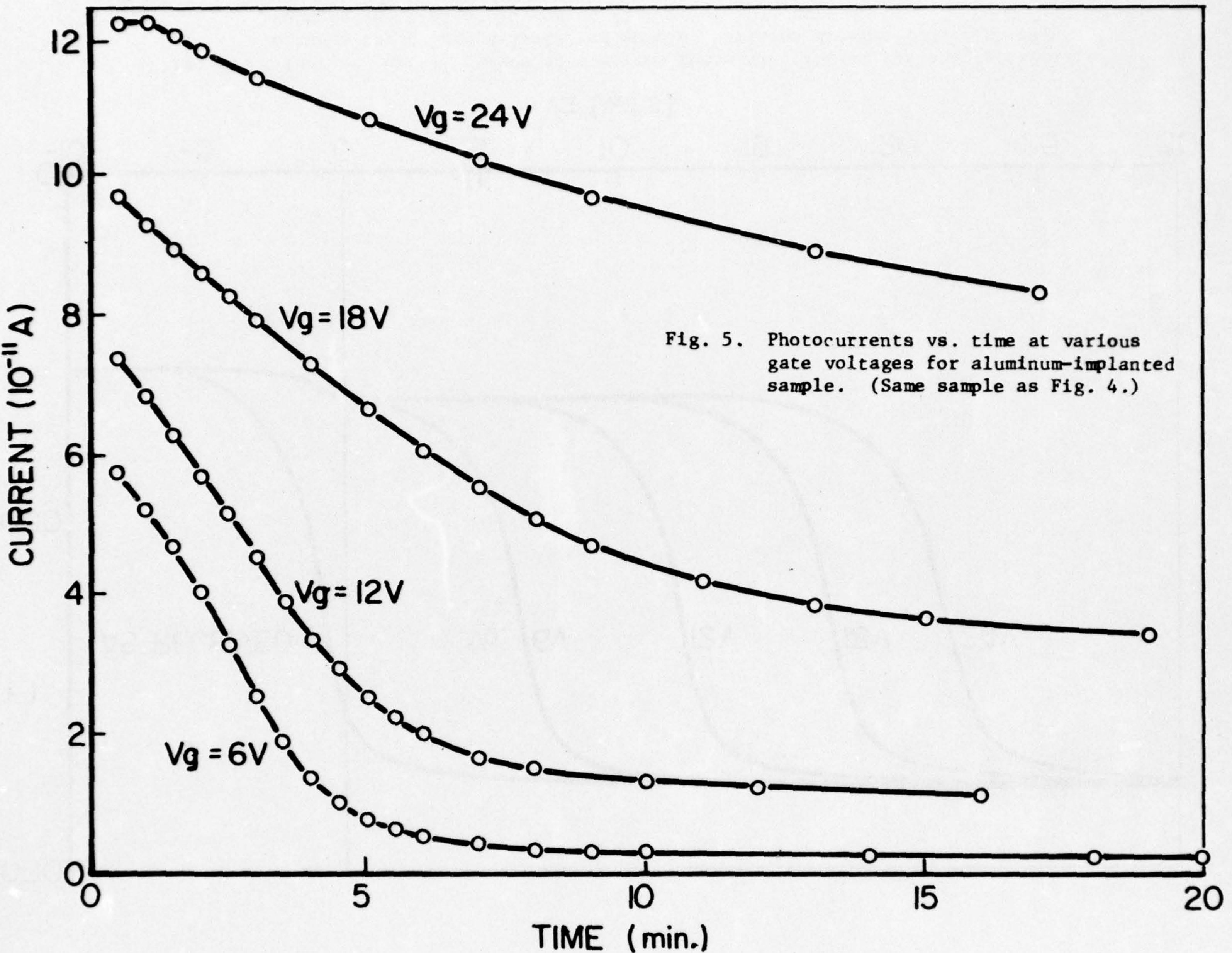

Fig. 5. Photocurrents vs. time at various gate voltages for aluminum-implanted sample. (Same sample as Fig. 4.)

than 6 V a substantial photocurrent continued to flow, showing that a conduction mechanism is important here that was not important in the more lightly implanted sample of Figs. 1 and 2. Essentially the same results were obtained at reduced temperature (128°C), indicating that the conduction mechanism which makes itself evident at the higher implantation fluences may be quantum-mechanical hopping between traps rather than thermionic (Poole-Frenkel) emission from traps.

Of central interest here, however, is the fact that essentially the same results as the above were obtained with the neon-implanted sample, as is shown by comparison of Figs. 6 and 7 with Figs. 4 and 5. The smaller currents seen in Fig. 7 as compared with Fig. 5 are not necessarily meaningful, for the alignment of the UV beam was not necessarily the same in the two cases. Also, the curve for V_g = 24 V is not useful because the sample broke down during the progress of this run. Our conclusion is that the neon-implanted sample, which presumably had only displacement damage to cause electronic activity, showed essentially the same features as the aluminum-implanted sample, and therefore that displacement damage contributed substantially to the electron trapping observed in the aluminum-implanted oxide.

As a further comparison between the effects of neon implantation and aluminum implantation, we examined the radiation sensitivity of both sets of unannealed samples. Figure 8 shows the results obtained with the aluminum-implanted sample. Curve 1 is the original C-V relationship. Irradiation with 2.5×10^5 rads (silicon) with a field plate voltage of + 10 V resulted in essentially no change. Curve 2 shows the effect of irradiation with 2.5 rads (silicon) at a field-plate voltage of -10 V. Further irradiation with an additional 1.5×10^5 rads at -10 V produced essentially no change in the curve. The sample was then biased with a field-plate voltage of +10 volts and exposed to 2.5×10^5 rads (silicon), resulting in Curve 3. Additional irradiation of 1.5×10^5 rads (silicon) at a field-plate voltage of +10 V produced Curve 4. The curves are somewhat stretched out after irradiation, presumably because of the generation of interface states, but the radiation hardness under positive field-plate voltage is evident.

Figure 9 shows the results obtained with a neon-implanted sample. Curve 1 is the original C-V characteristic. Curve 2 was obtained after X-irradiation of 2.5×10^5 rads (silicon) with the field plate at +10 V, and Curve 3 shows

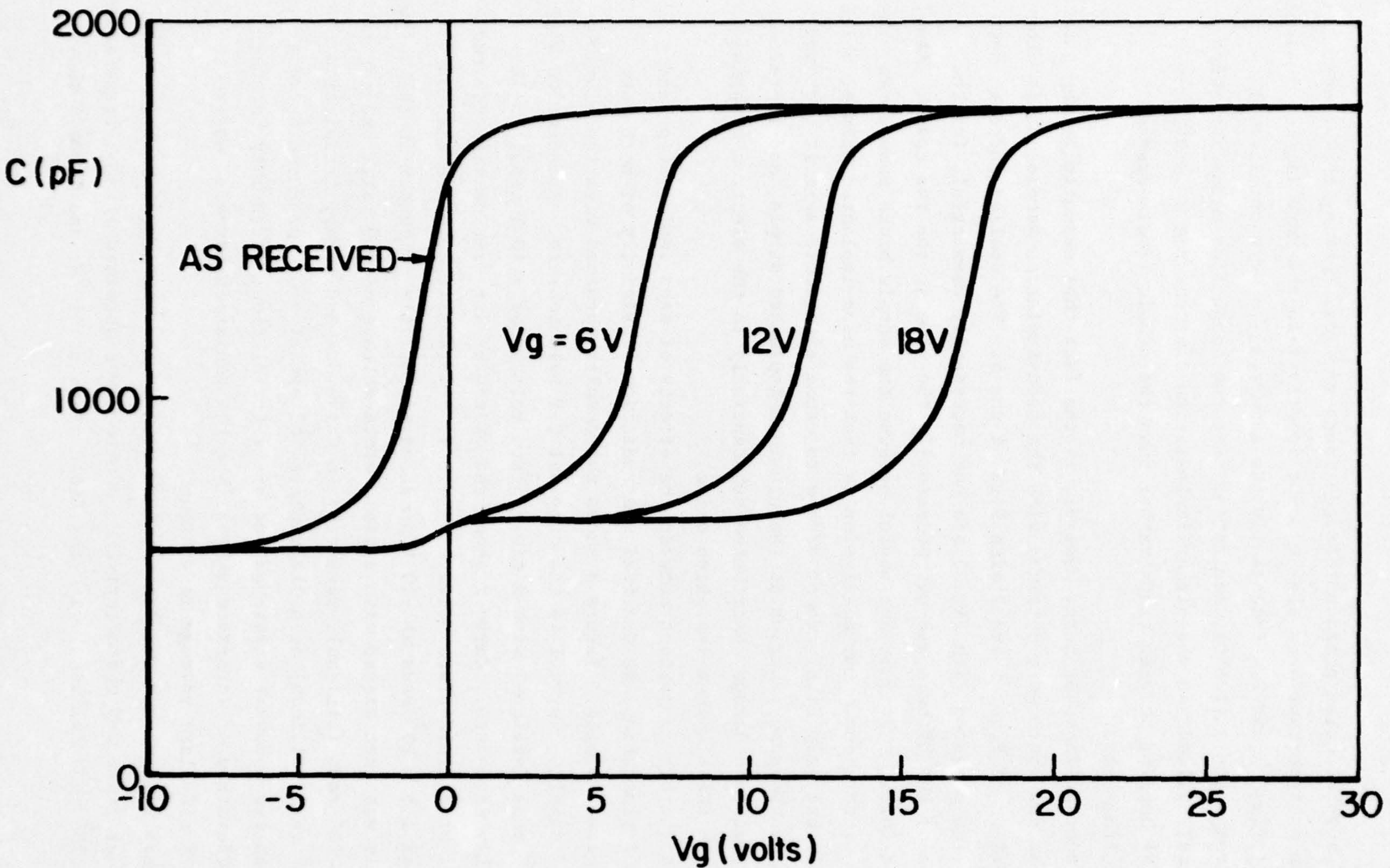

Fig. 6. For comparison with Fig. 4. Effect on C-V curves of electron photoinjection at various field-plate voltages for neon-implanted sample. Silicon dioxide 1000 Å thick, implanted with Ne at 20 keV to fluence of 1.5 x 10^{15} cm^{-2}. The sample broke down during the run at V_g = 24 V.

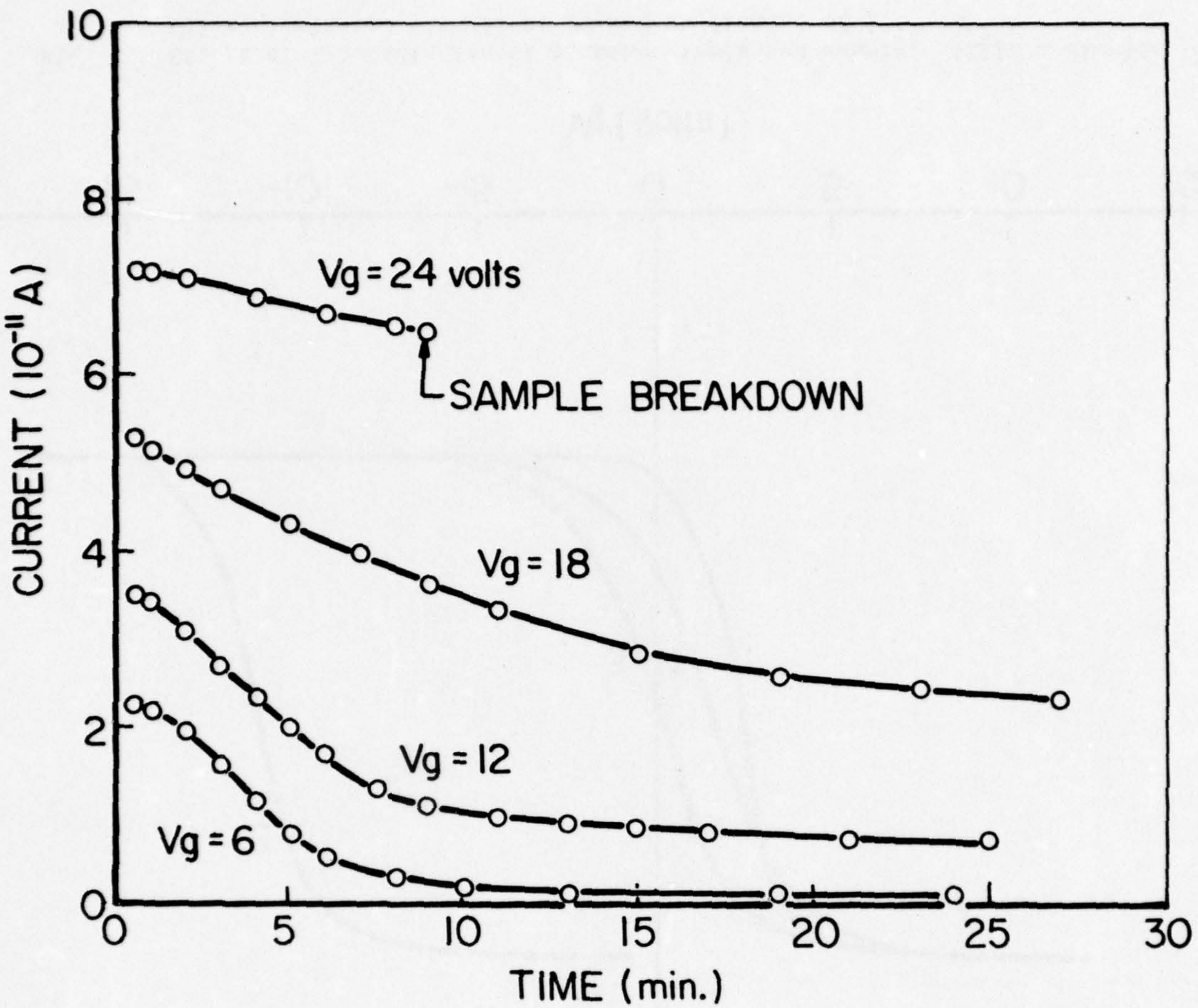

Fig. 7. Photocurrents vs. time at various gate for neon-implanted sample. (Same sample as Fig. 6.)

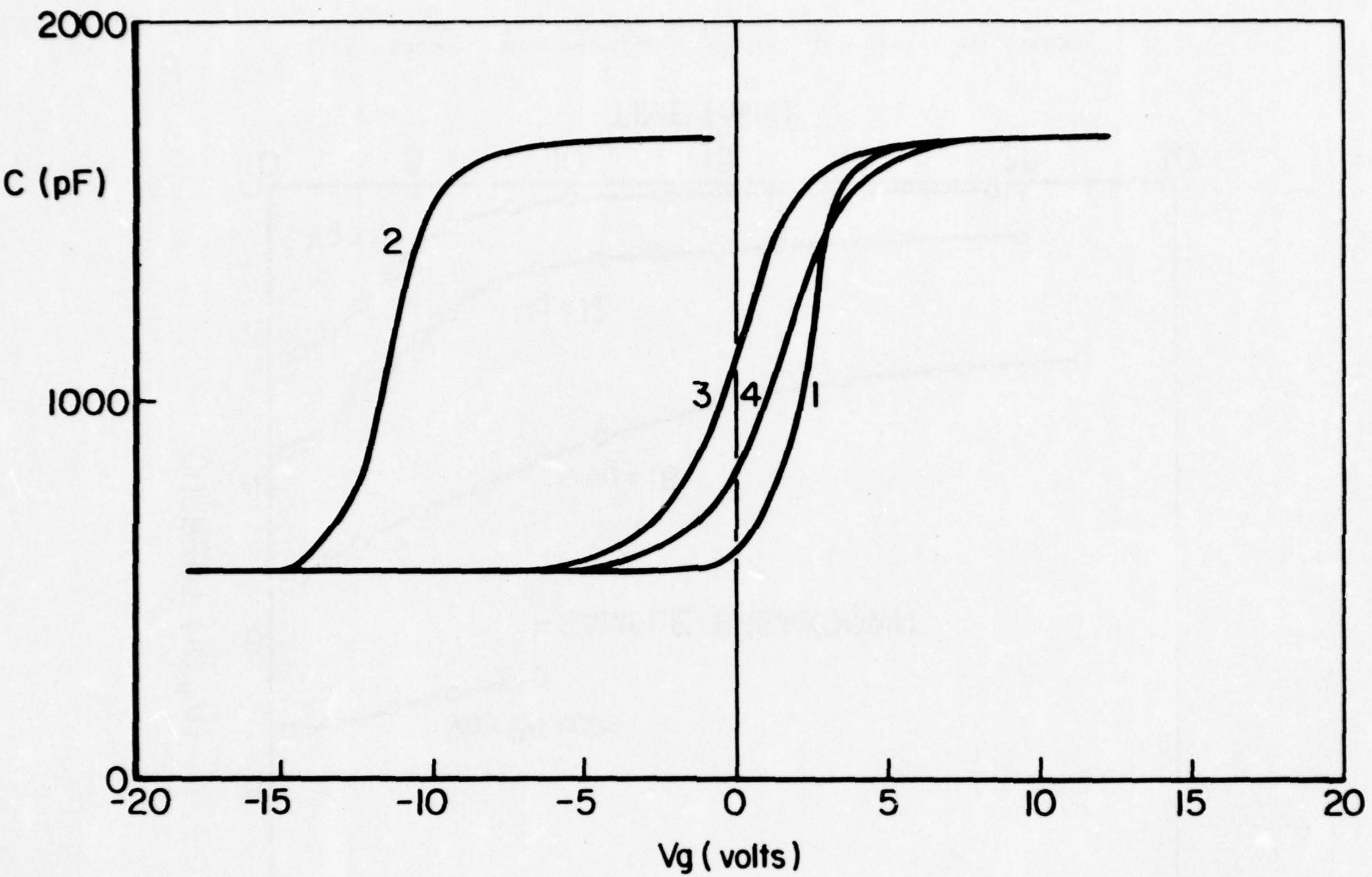

Fig. 8. Effect of X-irradiation of aluminum-implanted sample. Silicon dioxide 1000 Å thick, implanted with Al at 20 keV to fluence of 10^{15} cm^{-2}.

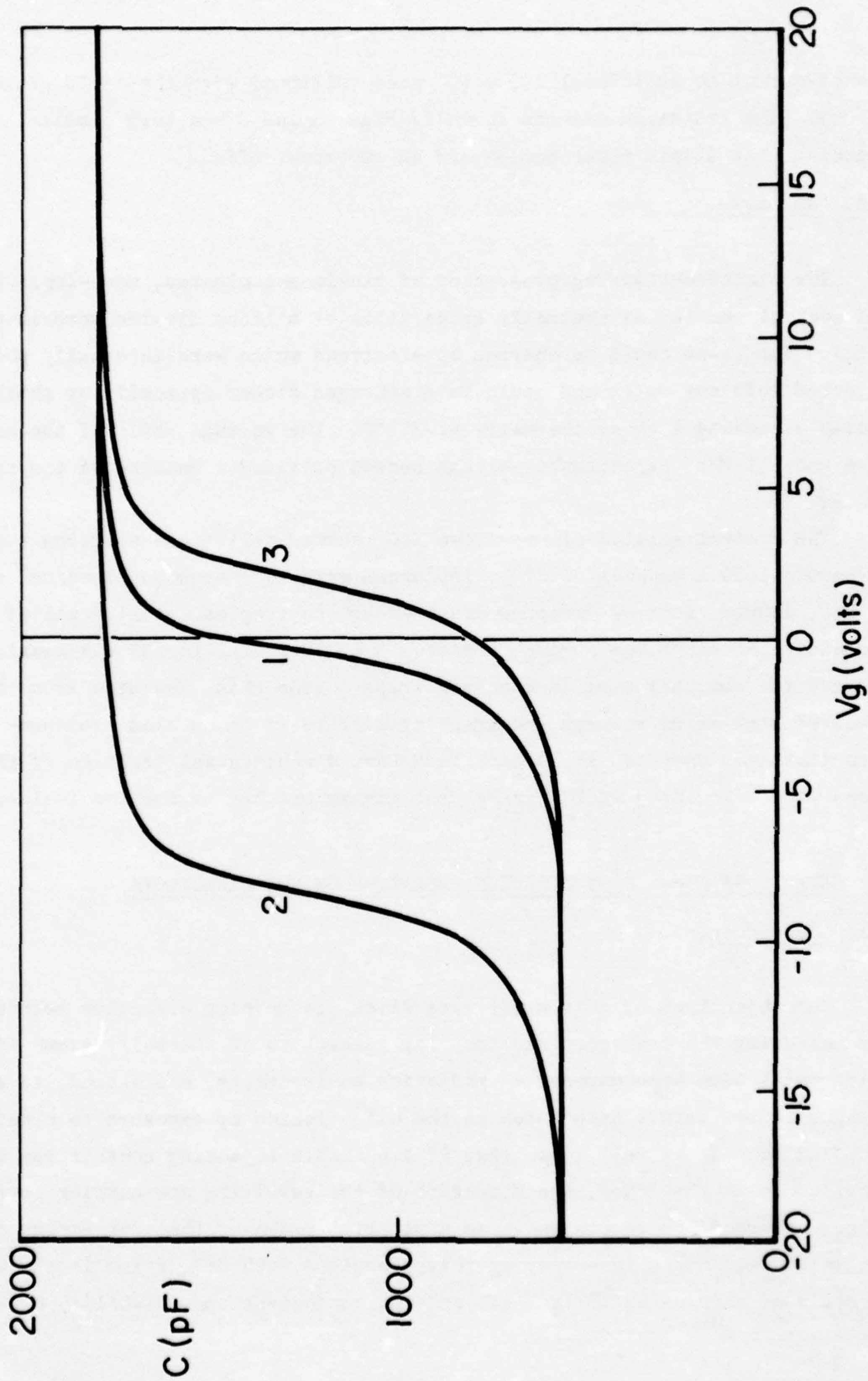

Fig. 9. For comparison with Fig. 8. Effect of X-irradiation of neon-implanted sample. Silicon dioxide 1000 Å thick, implanted with Ne at 20 keV to fluence of 1.5×10^{15} cm^{-2}.

the effect of an additional 1.5×10^5 rads (silicon) with the field plate at - 10 V. The radiation effects shown in Figs. 8 and 9 are very similar, indicating that displacement damage had an important effect.

2.5. Summary

The electron-trapping properties of aluminum-implanted, neon-implanted, and control samples of thermally grown films of silicon dioxide were investigated. The traps could be charged by electrons which were internally photoinjected into the oxide and could be discharged either optically by photons of energy exceeding 4 eV or thermally at 350°C. The voltage shift of the high-frequency (1 MHz) capacitance-voltage curves provided a measure of the trapped charge.

The control samples of dry-grown SiO_2 showed negligible electron trapping. Dry-grown 1400 Å samples of SiO_2, implanted with 10^{14} aluminum ions/cm^2 at 20 keV, showed electron trapping great enough to trap essentially all of the photoinjected electrons during transit. A 600°C anneal for 30 min considerably reduced the concentration of electron traps. From this, and also from an observed similarity between the trapping effects in unannealed aluminum- and neon-implanted samples, it is concluded that a substantial fraction of the traps were associated with displacement damage created by the ion implantation.

3. EFFECTS OF LOW-ENERGY ELECTRON RADIATION ON MOS CAPACITORS

3.1. Introduction

The objectives of this study were first, to develop effective methods for measuring the transport and trapping parameters of thermally grown SiO_2 films which have been exposed to radiation environments, and second, to study changes in the defect structures in the oxide following exposure to electron irradiation. It is well known that if a suitable injecting contact can be provided to an insulator, the structure of the resulting one-carrier current-voltage characteristic can serve as a powerful probe of the trap structure.[16] The major difficulty in employing this technique with SiO_2 films is the wide band gap of this material ($\sim$ 9 eV) and the consequent unavailability of any

conventional ohmic contact. This problem can be at least partially circumvented by using a low-energy electron beam to inject electrons just under the surface of the insulator, thus providing a quasi-ohmic contact. The silicon substrate, biased positively, serves as the anode. Curves of the relative rates of electron-beam energy deposition in SiO_2, based on the work of Everhart and Hoff,[17] are given in Fig. 10 for various electron beam energies. Two distance scales are shown, corresponding to aluminum field plates of two different thicknesses: 100 Å and 500 Å. It can be seen that with an aluminum field plate of 500 Å thickness, a 3 kV electron beam will dissipate almost all of its energy in the first 1000 Å of oxide. If an oxide of 5000 Å thickness is used in the experiment, the remaining 4000 Å of oxide will serve as the drift region for study of the transport and trapping properties of the insulator. Section 3.2 describes typical results obtained by use of this technique; Sec. 3.3 describes a study of the electron traps which are found to be generated in the SiO_2 by the electron-beam irradiation. Further details regarding these studies can be found in Reference 18.

3.2. Study of Electron-Beam-Induced Conduction in SiO_2

A typical set of results obtained in this study is shown in Fig. 11. The sample had a 4000 Å layer of SiO_2 which was grown at 1000°C in dry oxygen. The substrate was n-type silicon, (100) orientation, 1-5 ohm-cm resistivity. The field plate was of aluminum, 400 Å in thickness. The sample was bombarded through an aperture with a 2.8 kV electron beam which had normal incidence on the field plate. The field plate was grounded, and a positive voltage was applied to the substrate. The graphs of Fig. 11 show the steady-state J-V relationships obtained at room temperature with two different beam currents (open circles and solid circles) and at elevated temperature (100°C, triangles). The following features can be seen in these results:

(1) The J-V characteristic has two distinct regions: an ohmic region and a square-law region.

(2) The current at a given voltage is linearly proportional to the beam current.

(3) The current is essentially independent of the temperature.

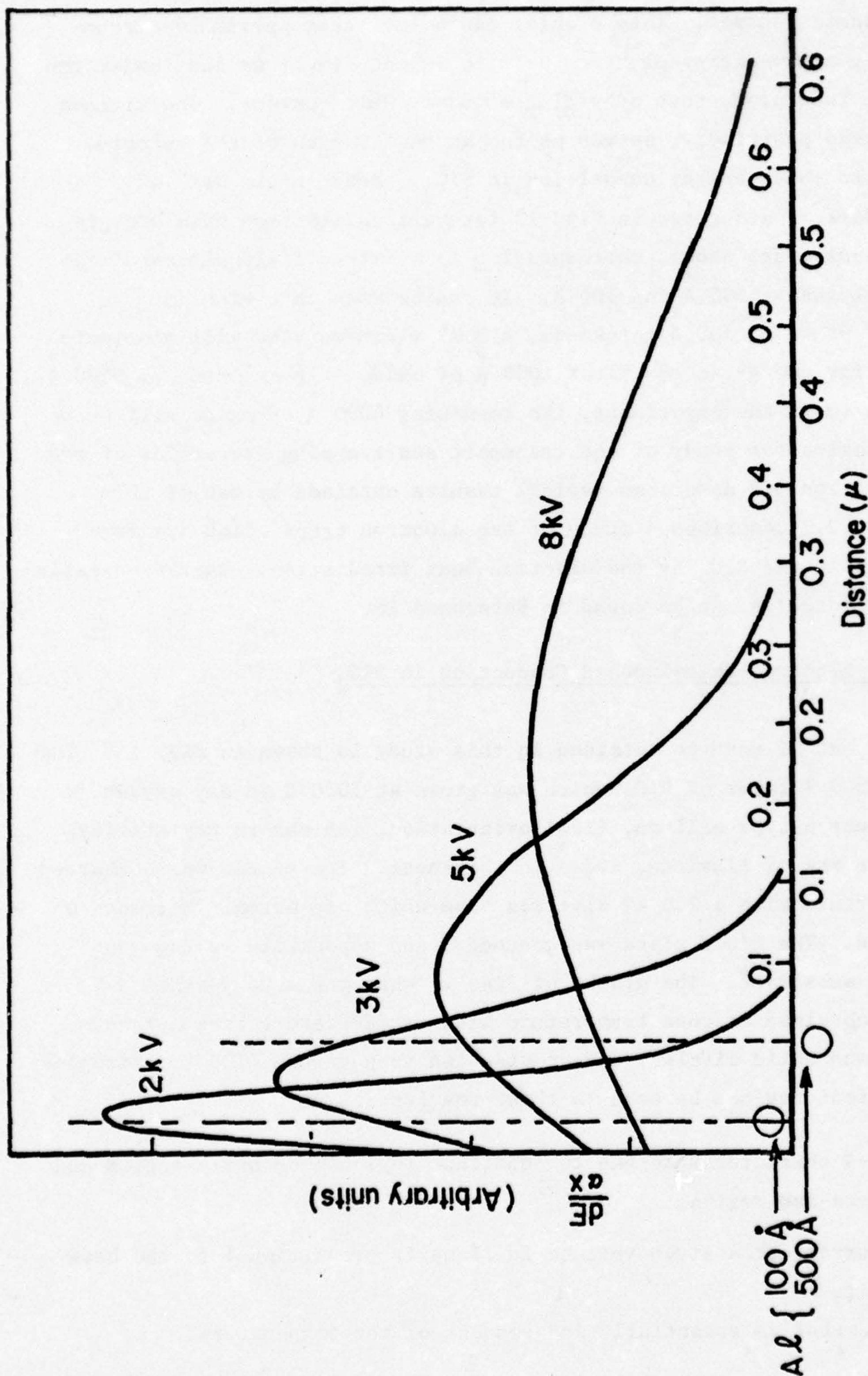

Fig. 10. Relative rate of energy deposition by electron beam in SiO_2.[17]

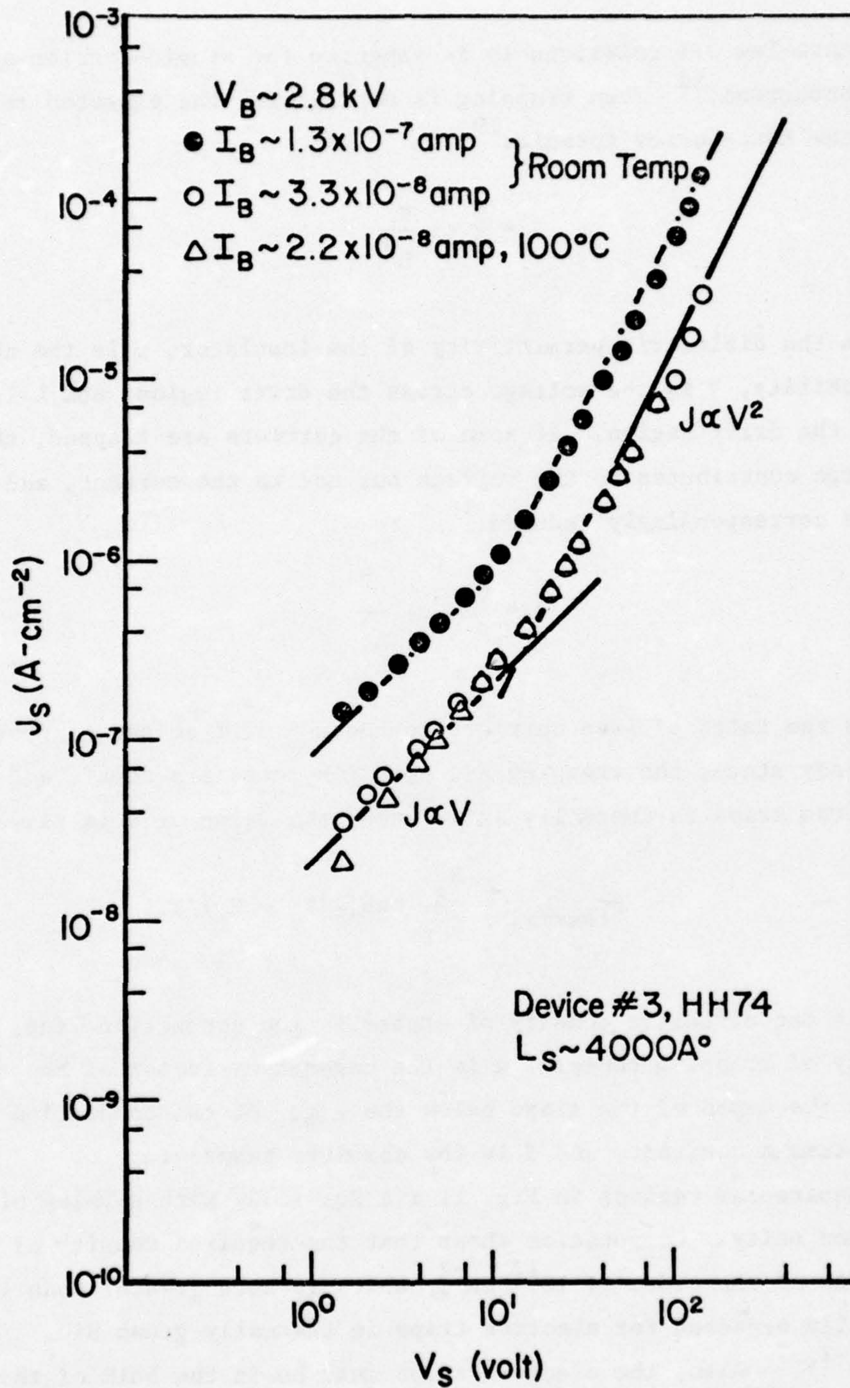

Fig. 11. Current-voltage characteristic for fixed beam voltage, two beam currents, and two temperatures.

A square-law J-V relationship is expected for single-carrier space-charge-limited conduction.[16] When trapping is negligible, the expected relationship is given by the Mott-Gurney formula:[19]

$$J = \frac{9}{8} \varepsilon\mu \frac{V^2}{L^3} \tag{3.1}$$

where ε is the dielectric permittivity of the insulator, μ is the charge-carrier mobility, V is the voltage across the drift region, and L is the length of the drift region. If some of the carriers are trapped, the trapped space charge contributes to the voltage but not to the current, and the current is correspondingly reduced:[16]

$$J = \frac{9}{8} \theta \varepsilon\mu \frac{V^2}{L^3} \tag{3.2}$$

where θ is the ratio of free carriers to the sum of free and trapped carriers. In the steady state, the trapping and emission rates are equal, and if the emission from traps is thermally stimulated, the value of θ is given by

$$\theta_{thermal} = \frac{N_g}{gN_t} \exp[-(E_c - E_t)/kT] \tag{3.3}$$

where N_c is the effective density of states in the conduction band, N_t is the density of trapping centers, g is the degeneracy factor of the traps, $E_c - E_t$ is the depth of the traps below the edge of the conduction band, k is the Boltzmann constant, and T is the absolute temperature.

The square-law regions in Fig. 11 fit Eq. (3.2) with a value of θ much smaller than unity. Computation shows that the required density of trapped electrons is of the order of 10^{17} cm^{-2}, which is much greater than the density normally expected for electron traps in thermally grown SiO_2 ($\sim 10^{14}$ cm^{-2}).[7] Also, the electron traps must be in the bulk of the oxide, not entirely at either interface. An interpretation of the foregoing result is that the shallow electron bombardment resulted in the generation of electron trapping centers in the bulk of the oxide, ahead of the range of the primary electrons themselves.

Substantiating evidence was as follows. Observation (2), namely that the current was linearly proportional to the electron-beam current, can be explained on the basis of photon-induced detrapping of trapped carriers, the photons being produced by the primary electrons in stopping. The flux of such photons, and the resulting rate of detrapping, would be proportional to the beam current. An alternative explanation, namely that the current was contact-limited, is inconsistent with the square-law characteristic, for $J \propto V^2$ is typical of space-charge limitation rather than contact limitation. Finally, Observation (3), namely that the current was independent of temperature, indicates that emission from the traps was not thermally induced. This is consistent with the interpretation in terms of photon-induced emission. The existence of an ohmic region preceding the square-law region, as seen in Fig. 11, is also consistent with the foregoing interpretation, for photons with energies considerably greater than the oxide band gap can penetrate through the oxide and generate hole-electron pairs in proportion to the beam current. The space-charge-limited square law is seen at higher voltages where the injection of carriers from the electron reservoir dominates over the pair production in the bulk.

In order to obtain independent evidence regarding the generation of electron traps by the electron irradiation, a further study of electron trapping was conducted, as described in the next section.

3.3. Study of Electron Traps Generated in SiO_2 by Electron-Beam Irradiation

In this study of electron trapping in electron-irradiated SiO_2, the traps in the oxide were charged by an internal photoinjection of electrons and were discharged thermally. The storage of trapped charge was determined from C-V curves measured at 1 MHz. The internal photoinjection was accomplished by biasing the field plate either positively or negatively depending on whether electron injection was desired from the substrate or from the field plate, and the structure was illuminated through the semi-transparent field plate with 4-eV photons.

Control samples showed negligible electron trapping (consistent with a concentration of electron traps on the order of 10^{14} cm^{-3}).

Figure 12 shows typical results obtained on a dry-grown oxide of 4700 Å thickness. The substrate was n-type silicon, (100) oriented), 1-5 ohm-cm resistivity. The field plate was aluminum, 150 Å in thickness. Curve 1 is the C-V curve of the sample before irradiation with electrons. Curve 2 shows the effect of irradiation with a 4.5 keV electron beam which deposited most of its energy within the first 2000 Å of the oxide. The dose of electrons was 7×10^{15} per cm^2. The stretch-out of the curve indicates the presence of interface states. Curve 3 shows the result of a one-hour anneal at 300°C which removed most of the interface states. The effect of negative charge storage, presumably in electron traps, is now shown clearly by the positive shift of flat-band voltage compared with Curve 1. Some electrons might, of course, have been removed from the traps by the anneal. Curve 4 shows the result obtained after photoinjecting electrons from the substrate into the SiO_2. Some of these electrons were trapped in the oxide, increasing the positive flat-band voltage shift. Curve 5 was obtained after an additional photoinjection of electrons, this time for the metal field plate. A small additional storage of negative charge is seen here. Computation shows that the negative trapped charge, if uniform, amounted to 4×10^{16} electrons/cm^3, which is at least two orders of magnitude greater than the negative trapped charge observed in the control samples under similar conditions.

As is shown by Curve 6 of Fig. 12, an anneal for 2 hrs at 350°C discharged the traps almost completely. The traps themselves remained after this treatment, however, for a further injection of electrons restored a positive flat-band shift similar to that shown by Curve 5 of Fig. 12. Alternate charging and discharging could be carried out repeatedly without causing any apparent reduction in the concentration of traps. The traps were deep, attempts at photodepopulation at photon energies up to 4 eV producing no appreciable effect. The stored charge was stable at room temperature over a period of days.

The original interpretation of the J-V curves, given in Sec. 3.2, required the traps to be distributed through the bulk of the oxide. To check this, the voltage dependence of photoemission was measured for samples which had been irradiated with electrons, then discharged by a thermal anneal, and finally recharged to saturation by electron photoinjection. When the bulk contains a negative space charge, a photoinjection of electrons will not occur

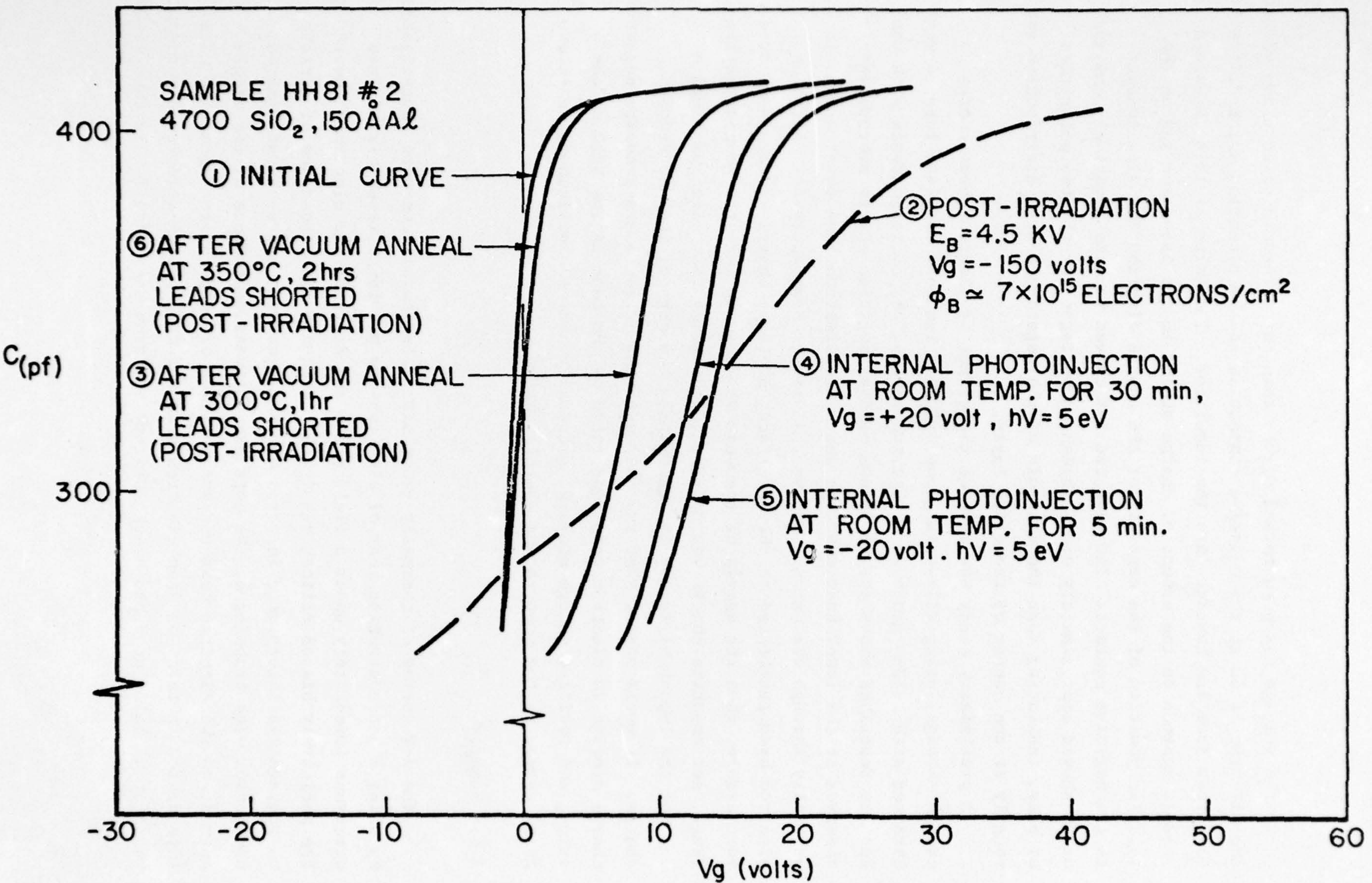

Fig. 12. Evidence of electron trapping in SiO_2 after irradiation by a nonpenetrating electron beam.

until the voltage has been raised higher than the threshold value above which the electric field at the negative contact is in the direction which drifts electrons from the contact into the insulator. The value of this threshold voltage depends on the amount of charge stored in the insulator and on the relative position of the centroid of the charge distribution with respect to the negative contact. The measured I-V curves for the negatively charged oxide showed approximately equal threshold voltages for the two polarities of bias, indicating that the centroid of the negative charge distribution was roughly at the center of the oxide layer.

A preliminary study was made of the effect of electron-beam energy on charge storage, using HCl-steam grown oxides. The most complete results were obtained with oxides grown on n-type substrates. In correspondence with the results described above for dry-grown oxides, negative charge storage was observed at the lower beam energies where the electron beam penetrated only partially through the oxide. However, at larger beam energies, where the electron beam penetrated to the interface, positive charge storage dominated. Furthermore, when the energy of the beam was reduced into the nonpenetrating range, net negative charge was restored, indicating that electron fluence was not the important factor in determining the sign of the net stored charge. It would appear that two charge-storage effects are present: negative charge storage in electron traps generated by the beam in the bulk of the oxide, and positive charge storage, presumably near the silicon-oxide interface, caused by the penetrating electron beam.

3.4. Summary

The J-V curves of thermally grown SiO_2 films on silicon were investigated by using a nonpenetrating beam of electrons to provide a reservoir of free electrons immediately under a field plate and drifting the electrons toward the positively biased silicon substrate. A square-law dependence of current on voltage was interpreted in terms of single-carrier space-charge-limited conduction with trapping of the carriers. Linear dependence of the sample current on the electron-beam current and lack of temperature dependence were interpreted in terms of deep electron trapping with photon-stimulated detrapping, the photons being produced by the primary electron beam itself. Further study

of the electron traps showed that they could be discharged by an anneal at 350°C for 2 hrs, and that they could subsequently be recharged by internally photoinjecting electrons from either electrode. The absence of similar electron trapping in control samples indicated that the electron-beam irradiation was responsible for generation of the electron traps.

Measurement of the positive and negative threshold voltages required to produce photocurrents through negatively charged oxides indicated that the centroid of the negative charge distribution was roughly at the center of the oxide layer, confirming an assumption made in the interpretation of the J-V curves. This indicates that the traps are generated through the bulk of the oxide, well ahead of the range of the primary electrons themselves.

4. STUDY OF LATERAL NONUNIFORMITIES AND INTERFACE STATES IN MIS STRUCTURES*

4.1. Introduction

For the past several years the semiconductor-insulator interface has been the subject of intensive study, first because it plays an important role in the characteristics of metal-insulator semiconductor (MIS) devices and secondly because it is the least understood part of the MIS structure. Capacitance-voltage (C-V) curves are an important diagnostic tool in the study of MIS structures. As is well known, the flatband voltage of an MIS capacitor, as deduced from a C-V curve, provides a convenient measure of the charge stored in the insulating layer. Commonly observed, however, is an abnormal stretch-out of the C-V curve along the voltage axis. Two entirely different mechanisms cause very similar stretch-outs: interface states, and lateral nonuniformities.[15] Interface states are those electronic states which exist at the semiconductor-insulator interface and can exchange charge with the semiconductor. Lateral nonuniformities include nonuniform insulator thickness, laterally nonuniform substrate doping, and, most commonly, nonuniform charge storage in the insulator. C-V stretch-out was originally attributed entirely to interface states, but it now seems likely that some of the problems were due instead to lateral nonuniformities,

---

* This study was performed by C. C. Chang[20] and was supported in part by the Bell Telephone Laboratories, Incorporated.

since the effects of the two on the C-V curves resemble each other. It is therefore important to identify the cause of C-V stretch-out correctly and to characterize the effect properly.

When an MIS structure is laterally uniform, and any C-V stretch-out is therefore caused only by interface states, the density of interface states as a function of energy can be obtained by any one of a number of well known and effective methods.[22-27] The situation regarding the identification and characterization of lateral nonuniformities is much less satisfactory. The study of the a-c conductance of MOS capacitors made by Nicollian and Goetzberger[27] indicated that a conductance measurement can be used to distinguish the effects of lateral nonuniformities from those of interface states. They related the area under the G/ω vs. ω curve to the density of interface states and interpreted the broadening of the conductance peak in terms of lateral nonuniformities. Castagne and Vapaille[26] used several C-V methods in an effort to determine the density of interface states of MOS capacitors after drifting ions to the Si-SiO_2 interface. They found that the different methods indicated different densities of interface states, and concluded that this discrepancy showed that the C-V stretch-out which they observed was due not to interface states but to lateral nonuniformities. Brews and Lopez[28] have suggested two methods, based on this principle, for testing for the presence of lateral nonuniformities.

In this work we have developed three new methods for distinguishing the effects of lateral nonuniformities from those of interface states. Two of the methods are based on the frequency dependence and temperature dependence, respectively, of the response of interface states. The third method is based on the principle (proved in Ref. 20) that if the C-V stretch-out is caused by lateral nonuniformities, the quasi-static and high-frequency C-V curves cannot both be fitted simultaneously by any distribution of interface states. The converse of this statement is also true. The convenient application of this principle makes use of a new and simple method that we have developed for the determination of the distribution of flatband voltages in an MIS structure that has a nonuniform charge storage.

As our model of a laterally nonuniform MOS capacitor we have taken a parallel combination of noninteracting small capacitors, each of which

can be considered to be uniform over a small characteristic area. As Brews[29] has pointed out, this model will not provide an accurate representation for lateral nonuniformities of small dimensions (e.g., individual ions) that are laterally well separated. In addition, Gordon[30] has shown that in the inversion regime the individual elementary capacitors interact at their edges through the minority carriers of the inversion layer. Despite these faults, the parallel-capacitor model is a reasonable first-order representation and has the advantage of being more readily amenable to analysis than the more complex representations.

4.2. Frequency Method

As is discussed in some detail in Ref. 20, the C-V relationship of an MIS capacitor without interface states is frequency-independent from approximately 100 Hz up to the majority-carrier ohmic relaxation frequency of perhaps 10^{12} Hz. In contrast with this, interface states near the center of the silicon bandgap have response times on the order of a millisecond, and in the depletion regime the interface-state capacitance will show a frequency dependence over a range from perhaps 100 Hz to 1 MHz, i.e., within the range of easy measurement. An example of this is shown in Fig. 13 for an MOS capacitor in which interface states had been generated by subjecting the oxide to a high electric field. The frequency dispersion of the "high-frequency" C-V curves shows the presence of the interface states. By contrast, Curve 1 of Fig. 14 was taken on a sample with negligible interface states but having a laterally nonuniform charge storage caused by bombarding the sample with a low-energy nonpenetrating electron beam, after which the sample as annealed at 350°C for one hour. The nonuniformity of charge storage was caused by spatial nonuniformity of the bombarding electron beam. Virtually identical C-V curves were obtained at measuring frequencies of 1 kHz, 10 kHz, 100 kHz, and 1 MHz. Calculated ideal C-V curves are shown by dashed lines for comparison. The departure of Curve 1 from the ideal, together with the lack of frequency dependence, shows the presence of lateral nonuniformities.

The frequency method actually detects interface states rather than lateral nonuniformities, and one can not be sure whether an observed

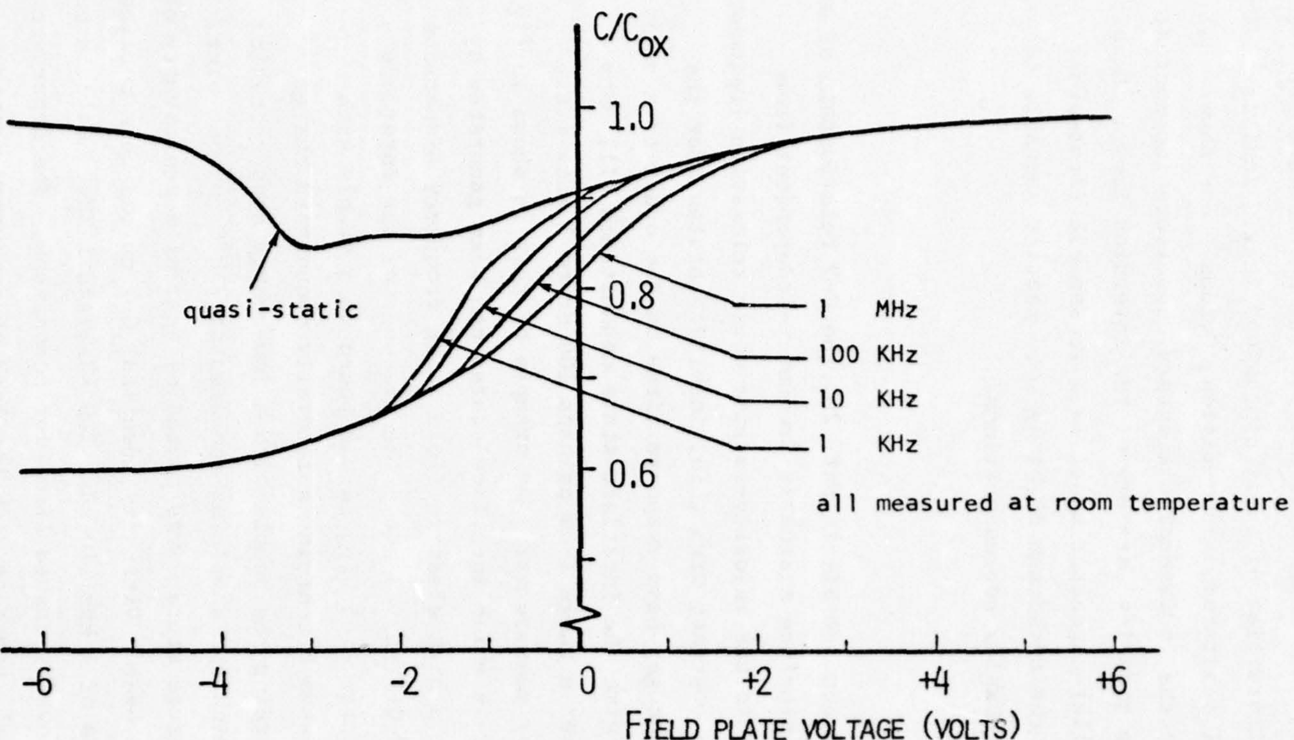

Fig. 13. C-V frequency dependence caused by interface states. Substrate: (100) n-Si, 1-2 ohm-cm. Silicon Dioxide: HCl-steam grown, 2560 Å. Interface states were generated by subjecting the oxide to an electric field of 6.8 MV/cm for 10 hrs at room temperature, field plate negative.

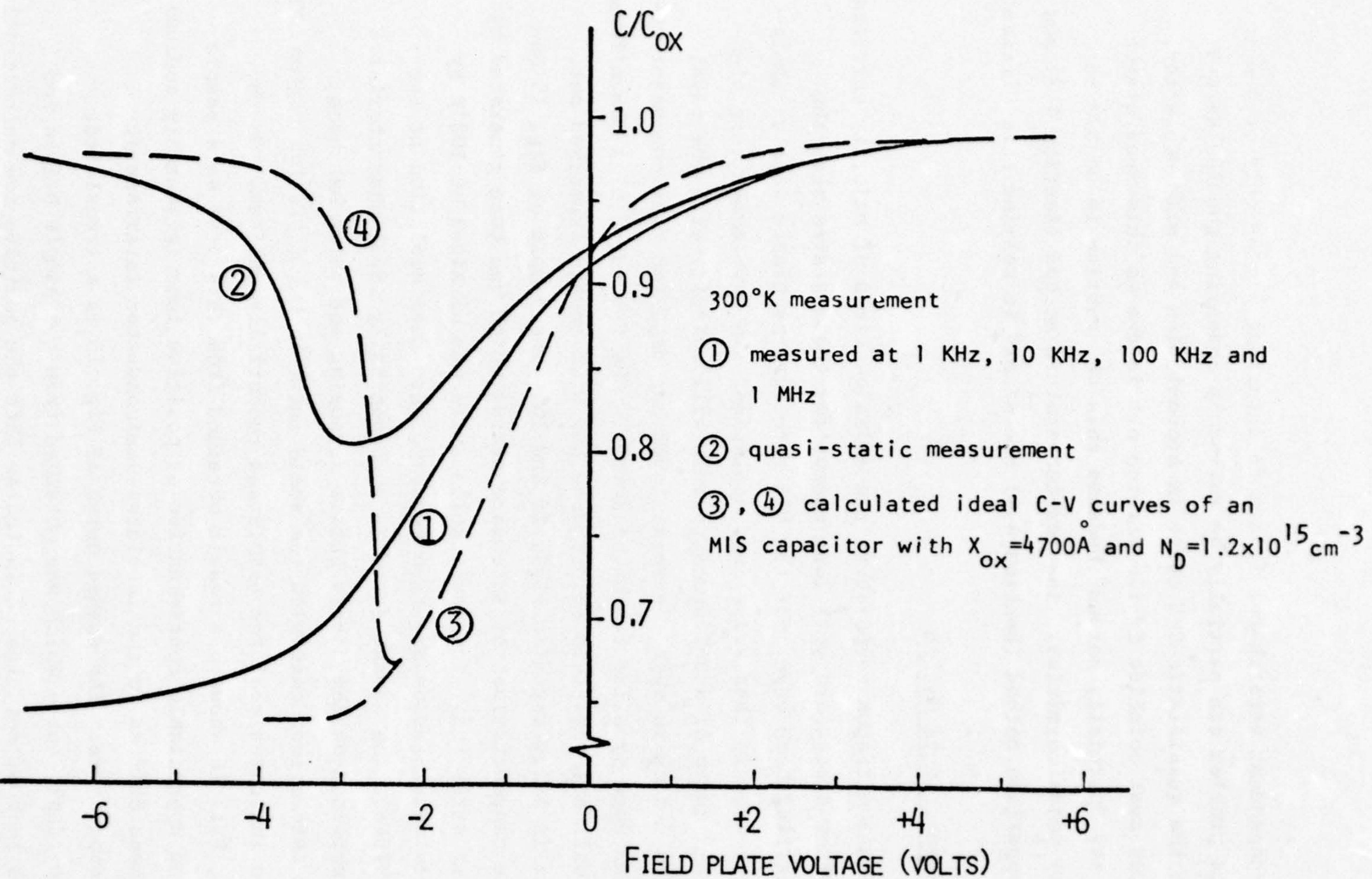

Fig. 14. Showing the frequency independence of the C-V curves of an MOS capacitor with laterally nonuniform charge storage. The dashed curves are calculated ideal C-V characteristics. Substrate resistivity 3-5 ohm cm, oxide thickness 4700 Å.

frequency-dependent stretch-out is due to interface states only or due to both. This problem can partially be solved by comparing the 100 Hz C-V curve with the quasistatic C-V curve in accumulation and mild depletion; these curves must coincide if the stretch-out is due to interface states only. We say "partially solved" because this observation is unable to detect tiny nonuniformities. The low-temperature method (Section 4.3) and the C-V comparison method (Section 4.4) are of aid in solving this difficulty.

4.3. Low-Temperature Method

At liquid nitrogen temperature the emission times of majority carriers from interface states are very long except for those states near the majority-carrier band edge. If the MIS structure is biased into accumulation and the bias is then swept into depletion, the low-temperature high-frequency C-V curve of a uniform structure will coincide with the ideal (translated) C-V curve when the Fermi level has departed from the majority-carrier band edge by a few tenths of a volt. The C-V curve of a nonuniform capacitor will not show this coincidence but will remain stretched out. This effect is illustrated in Figs. 15 and 16. The sample of Fig. 15 had appreciable concentrations of interface states which had been generated by high-voltage stressing. The lower solid curve was obtained at 100°K by biasing into accumulation and then sweeping into deep depletion at the rate of 5 V/sec. The dashed curve is an essentially ideal characteristic which was obtained on the sample before stressing and which has been translated into coincidence with the solid curve in the depletion region. This coincidence indicates that the sample was essentially uniform. On the other hand, Fig. 16 shows the result obtained from this test on a sample which had an appreciable contamination of positive ions (presumably sodium) which had been drifted to the insulator-semiconductor interface at elevated temperature. The dashed curve of Fig. 16 is a translated, essentially ideal, curve which was obtained from the sample before ion drift. The lack of coincidence indicates that the positive ion concentration at the interface is nonuniform.

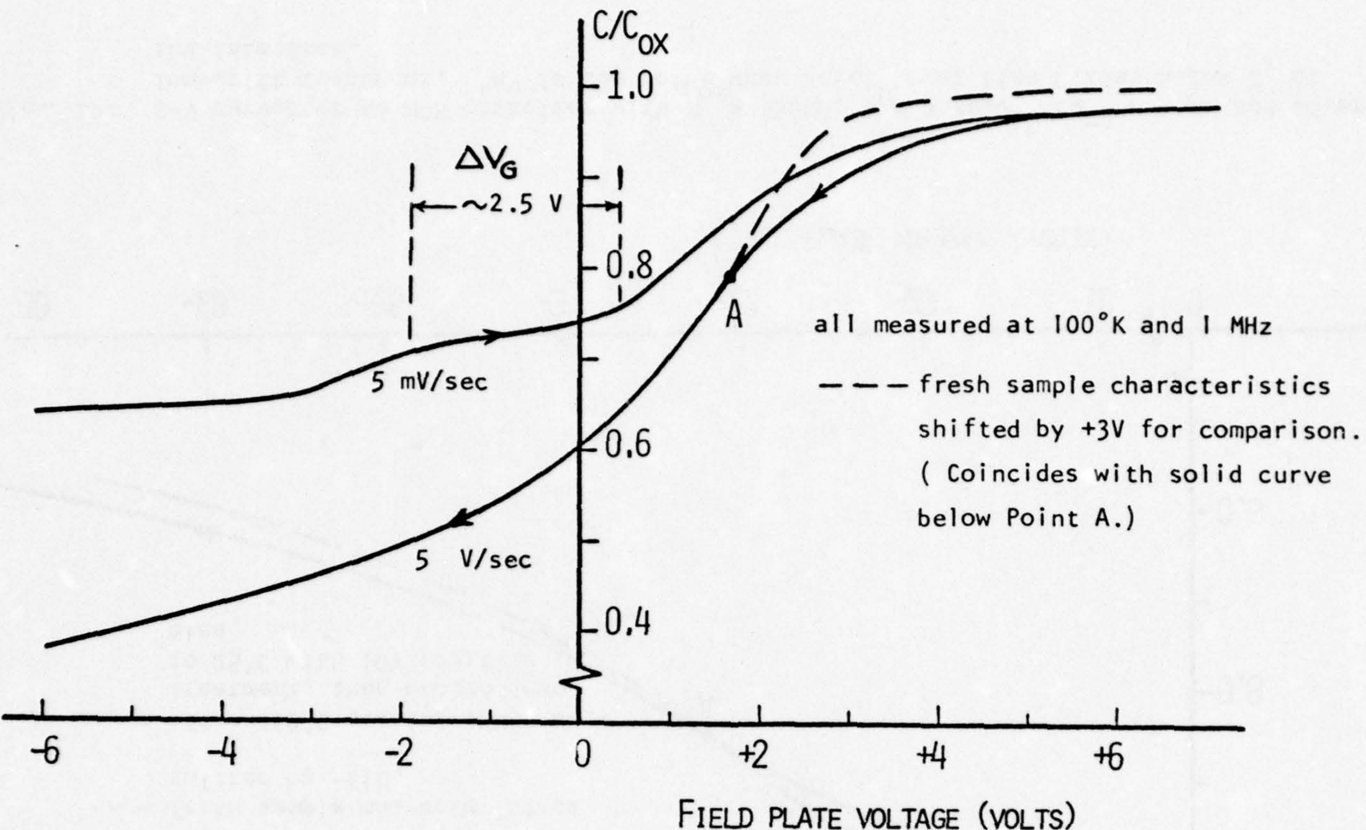

Fig. 15. C-V curves of an MOS sample with same specifications as that used in Fig.13 after gate(-) 175V 6 hrs. electrical stressing at room temperature. The point A corresponds to the condition when the Fermi-level lies 0.25eV below E_c at the interface.

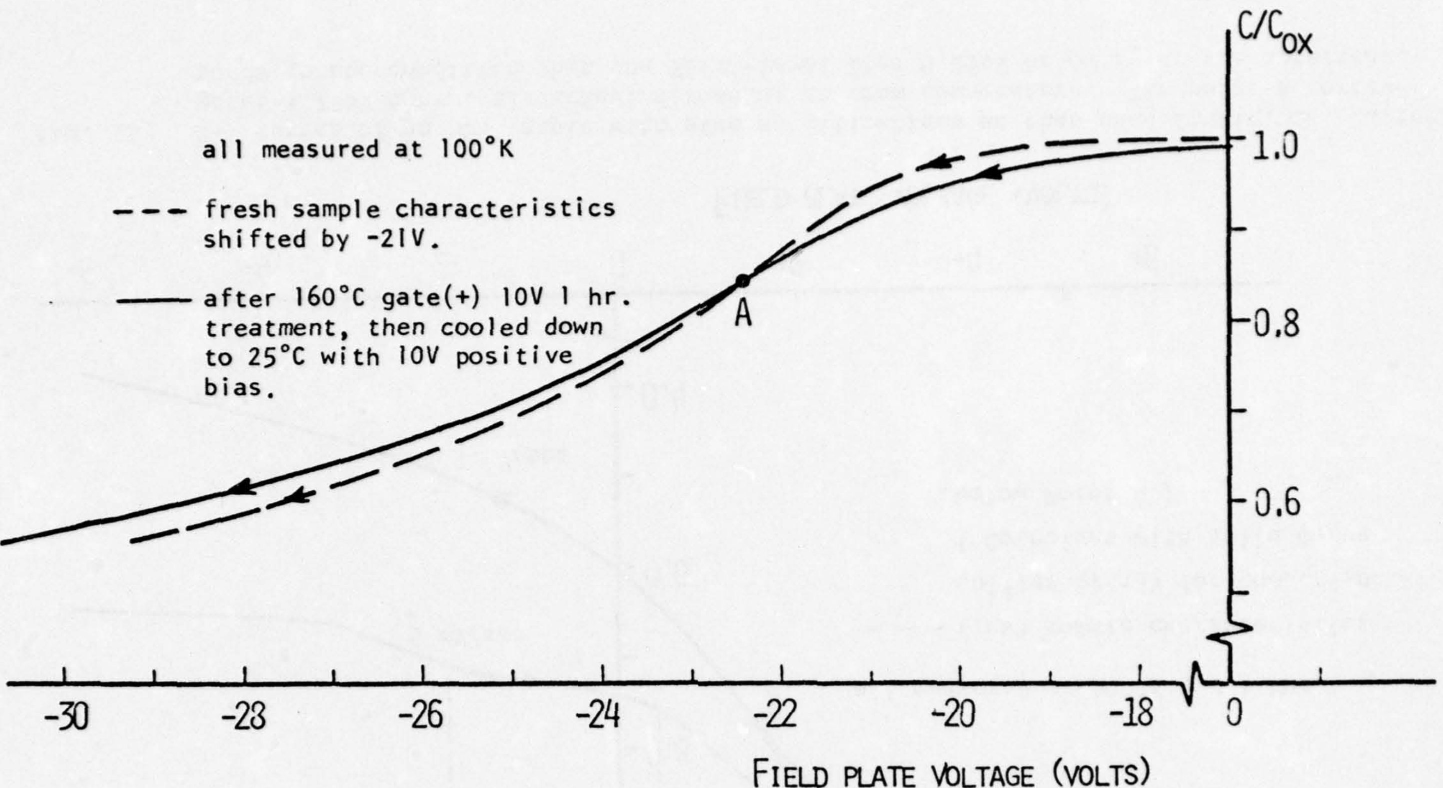

Fig. 16. C-V curves of an MOS capacitor with $X_{ox} = 3500\mathring{A}$, $N_D = 3.7\times10^{15}\ cm^{-3}$ before and after ion-drift treatment. "A" is the point when Fermi level lies 0.25eV below E_c at the interface.

A further low-temperature test, illustrated by the upper curve in Fig. 15, is useful when interface states are present. When the lower curve has been completed, the sample is brought out of deep depletion by temporary illumination. This process fills the interface states with minority carriers. The gate voltage is then swept slowly toward accumulation. When the density of majority carriers at the interface becomes appreciable, the interface states begin to fill with these carriers, causing a ledge in the characteristic.[20,31] The average density of interface states in (roughly) the lower half of the gap can be estimated from $\Delta V_g C_{ox}/q$, where ΔV_g is the width of the ledge. From Fig. 15 this estimate yields the density 2×10^{11} cm^{-2}.

4.4. C-V Comparison Method

The comparison method that we propose is based on the principle (proved in Ref. 20) that when a C-V stretch-out is caused by lateral nonuniformities, the resulting quasistatic and high-frequency C-V curves cannot both be fitted by any distribution of interface states, and, conversely, if the stretch-out is caused by interface states, the resulting quasistatic and high-frequency C-V curves cannot both be fitted by any lateral distribution of flatband voltages. The convenient application of this principle utilizes the method for determination of the distribution of flatband voltages presented in Section 4.5.

A convenient method for utilizing the foregoing principle is to perform a combination of two tests, as follows:

1. Test for lateral nonuniformities by assuming the opposite, i.e., assume that all the stretch-out is due to interface states. Then: (a) obtain the surface potential $\phi(V_G)$ by Berglund's method,[24] (b) from this result compute the corresponding high-frequency curve $C_{HF}(\phi(V_G))$, and (c) compare the computed C_{HF}-V curve with the measured $\check{C}_{HF}$-V curve. A mismatch between the two will indicate the presence of lateral nonuniformities.

2. Test for interface states by assuming the opposite, i.e., assume that all the stretch-out is due to lateral nonuniformities. Then: (a) determine the distribution of flatband voltages from the measured quasi-static and high-frequency C-V curves by the method described in Sec. 4.5 (this method is restricted to nonuniform charge storage, but this is the most common case), (b) using this hypothetical distribution of flatband voltages, regenerate the two C-V curves by computer, and (c) compare the two regenerated curves with the measured curves. A discrepancy indicates the presence of interface states.

Two examples will now be presented, one for a sample with interface states and the other for a sample with lateral nonuniformities.

The solid curves of Fig. 17 are the quasi-static and high-frequency (1 MHz) C-V curves for a sample in which interface states had been generated by high-field stress (same sample as in Fig. 13). We test for interface states by assuming the opposite. By use of the method of Sec. 4.5 we compute the hypothetical distribution of flat-band voltages caused by lateral nonuniformities. The resulting distribution, shown in Fig. 18, is then used in a computer-regeneration of the C-V curves, yielding the results shown by the dotted curves of Fig. 17. The considerable mismatch between these and the measured C-V curves indicates the presence of substantial concentrations of interface states.

Next, we apply the test for lateral nonuniformities by again assuming the opposite condition. The dotted curve in Fig. 19 is the high-frequency relationship calculated from the quasi-static curve under the assumption that the stretch-out is entirely due to interface states. The close agreement between the measured and computed high-frequency C-V curves indicates that lateral nonuniformities are negligible in this sample.

Figures 20 and 21 show the results obtained with a sample that had been bombarded with a nonuniform electron beam to produce a nonuniform storage of charge. First we assume the distortion to be due entirely to lateral nonuniformities, and use the quasi-static and high-frequency curves

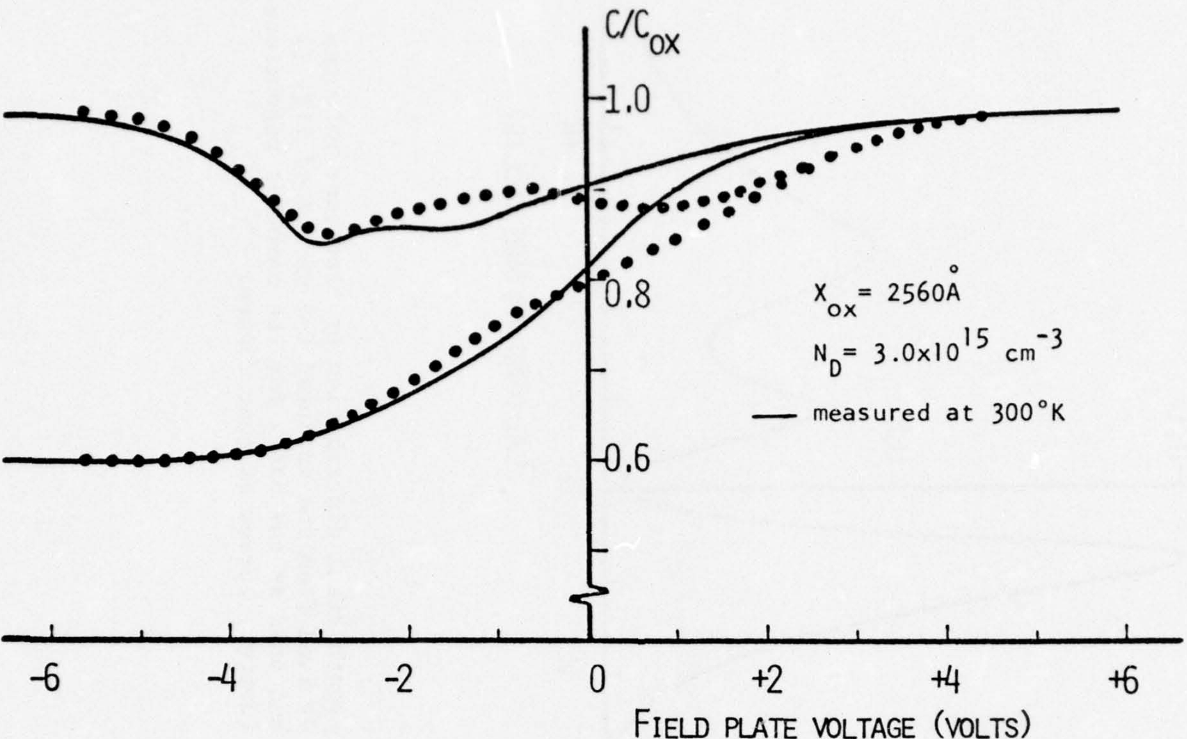

Fig. 17. Solid lines: Measured quasi-static and 1 MHz C-V curves.
Dots: Computer-regenerated curves obtained by using the comparison test for interface states. The mismatch indicates that interface states are present.

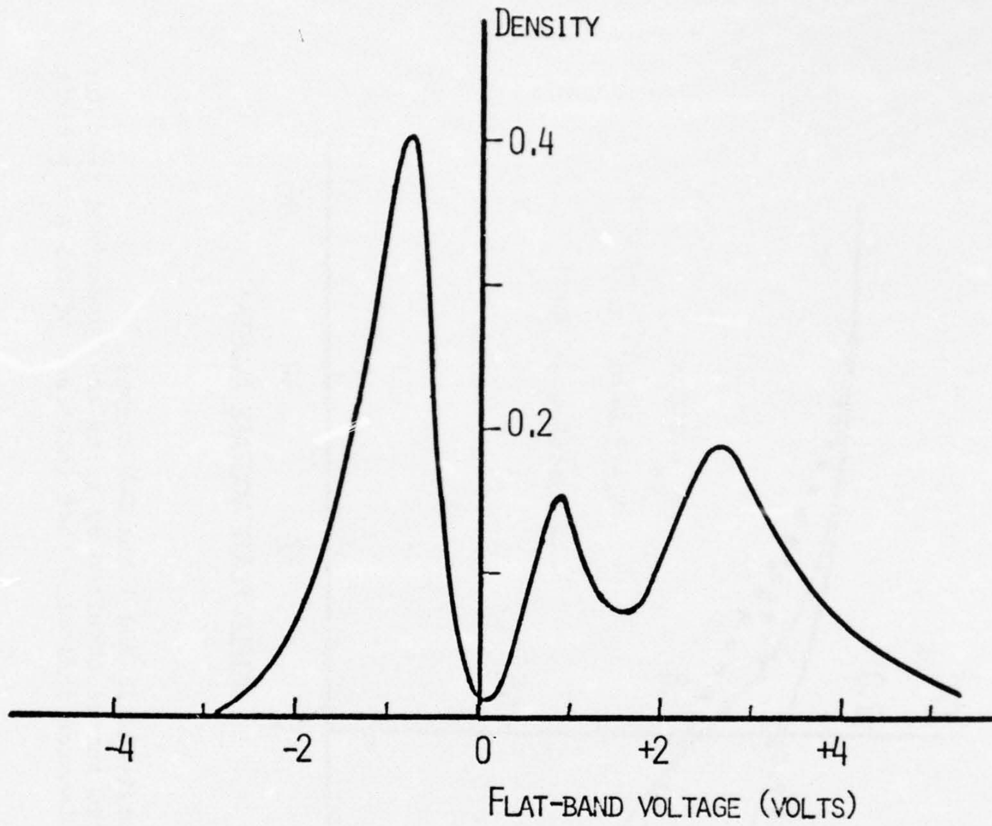

Fig. 18. Hypothetical distribution of flat-band voltages derived from the measured C-V curves of Fig. 17 and used as the basis for the computer-regenerated (dotted) curves of that figure.

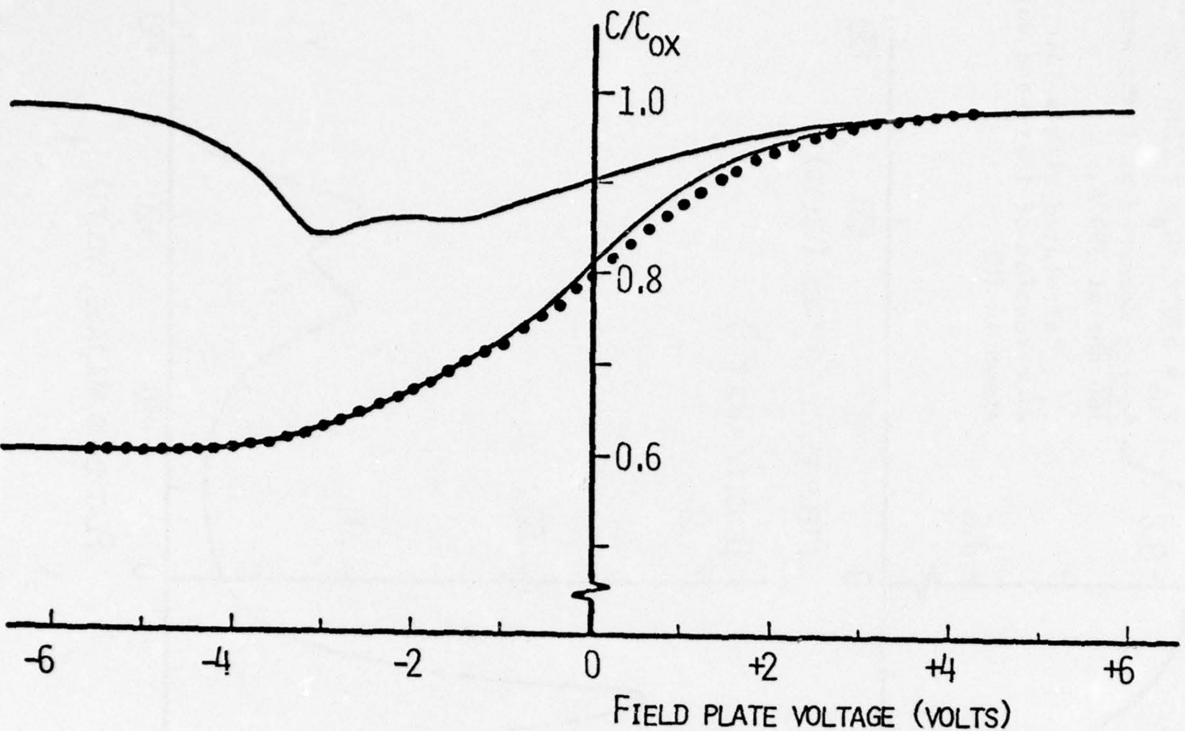

Fig. 19. Solid lines: Measured quasi-static and 1 MHz C-V curves (the same as in Fig.17). Dots: Computed high-frequency curve obtained using the comparison test for lateral nonuniformities. The close agreement between the measured and computed high-frequency curves indicates that lateral nonuniformities are negligible.

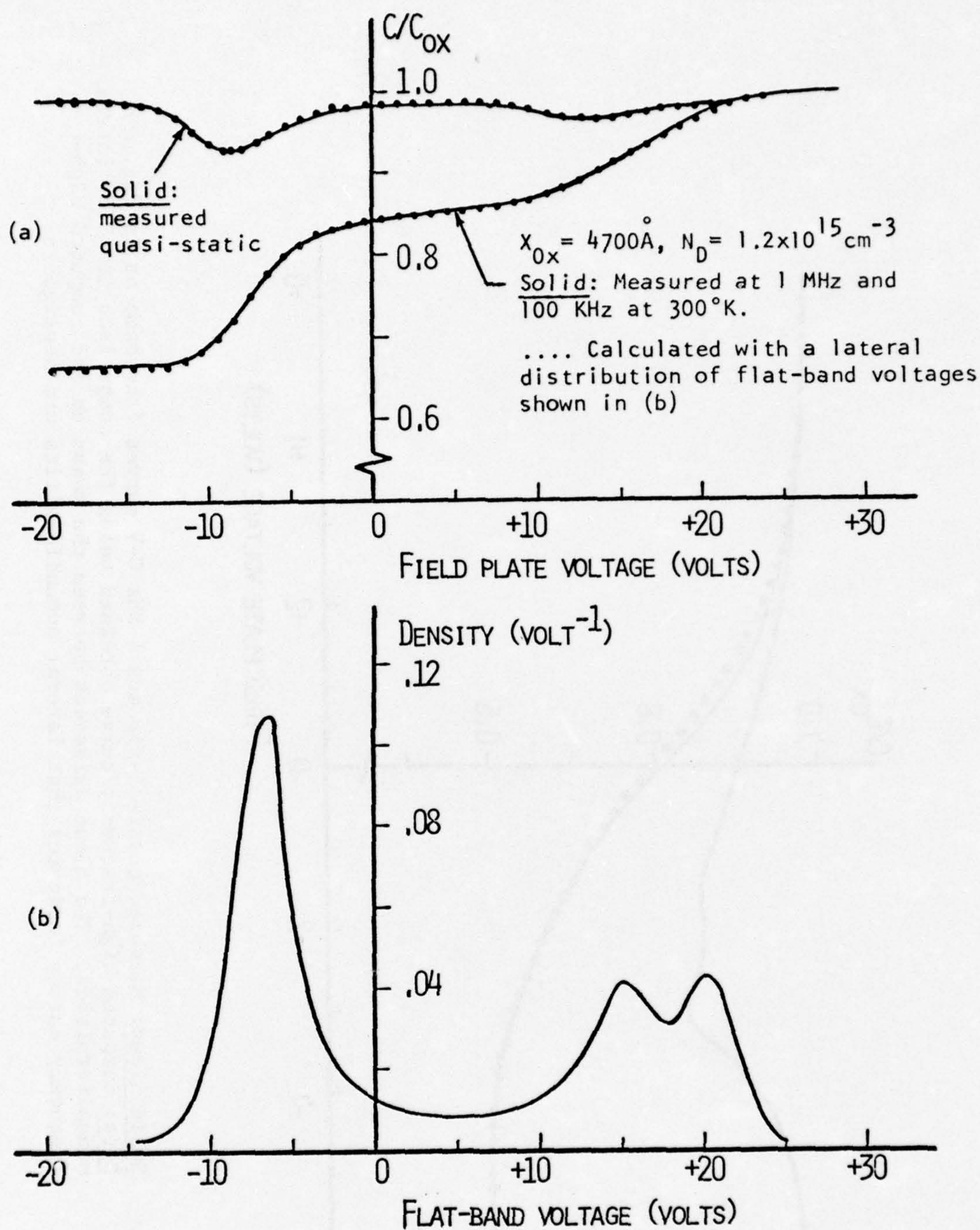

Fig. 20. (a) Measured (solid lines) and calculated (dots) C-V curves. (b) Lateral distribution of flat-band voltages determined from the measured curves of (a) by the method described in Sec. 4.5.

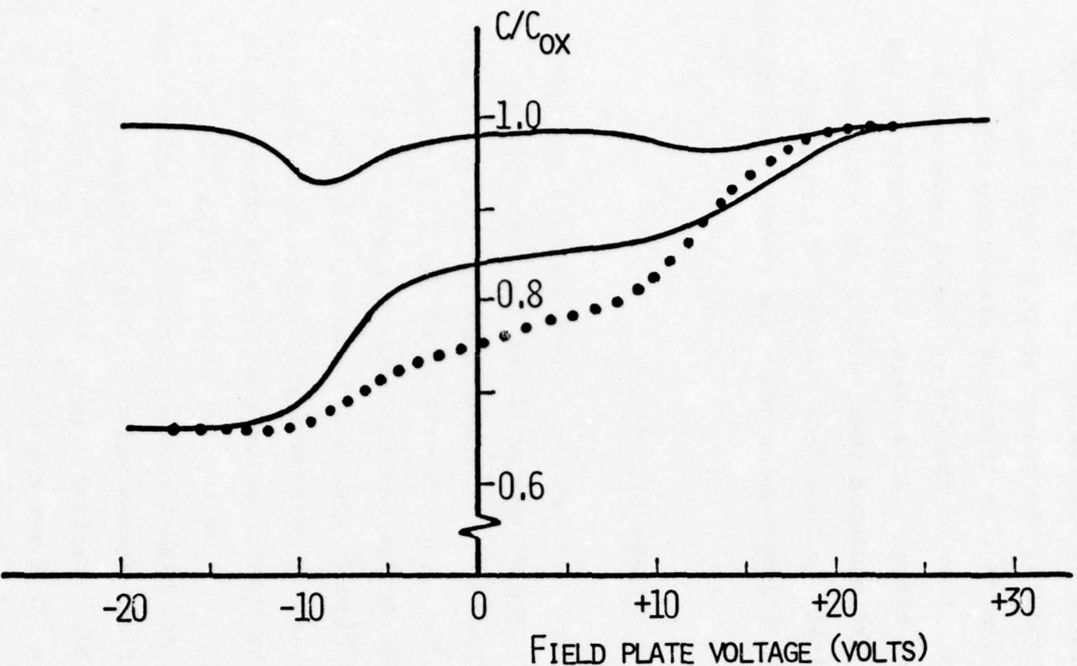

Fig. 21. Solid lines: Measured quasi-static and 1 MHz C-V curves [the same as those of Fig. 20(a)].

Dots: Computed high-frequency curve obtained using the lateral-nonuniformities test procedure. The lack of correspondence shows the presence of lateral nonuniformities.

[solid lines of Fig. 20(a)] to determine the corresponding distribution of flatband voltages, thus yielding the results of Fig. 20(b). From this distribution of flat-band voltages we then compute the quasi-static and high-frequency curves, thus obtaining the points shown by dots in Fig. 20(a). The correspondence indicates that interface states are not important and that the observed distortion of the C-V curves is caused by a laterally nonuniform storage of charge. As a check, we also compute the high-frequency C-V curve from the measured quasi-static curve assuming the stretch-out to be due entirely to interface states. The result is shown in Fig. 21. The lack of correspondence shows the presence of lateral nonuniformities.

4.5. Determination of Flatband Voltage Distribution

In this section we restrict our attention to MIS capacitors which have a laterally nonuniform storage of charge in the insulator but are otherwise uniform (insulator thickness, substrate doping), and which have negligible interface states. The objective will be to devise a method for determining the lateral distribution of flatband voltages from the stretched-out quasi-static and high-frequency C-V curves, using the parallel-array model. The problem is mathematically intractable unless approximations are made, and the approximation that we have chosen can be understood with the aid of Fig. 22. The top two graphs of Fig. 22 represent typical quasi-static and high-frequency curves for a uniform MIS capacitor with negligible interface states and a flatband voltage V_{FB} (actually computed for a p-Si MOS capacitor with $N_A = 5 \times 10^{15}$ cm^{-3} and $x_{ox} = 1000$ Å). Part (b) of Fig. 22 shows the distribution function of flatband voltages, this being a delta function of unit area. Part (c) of Fig. 22 shows the difference between the two capacitance functions: $C_{QS}(V_G) - C_{HF}(V_G)$. This difference is essentially zero for gate voltages smaller than $V_{FB} + V_T$, where V_T is the turn-on voltage of an ideal MIS capacitor having the same insulator thickness and substrate doping.[32]

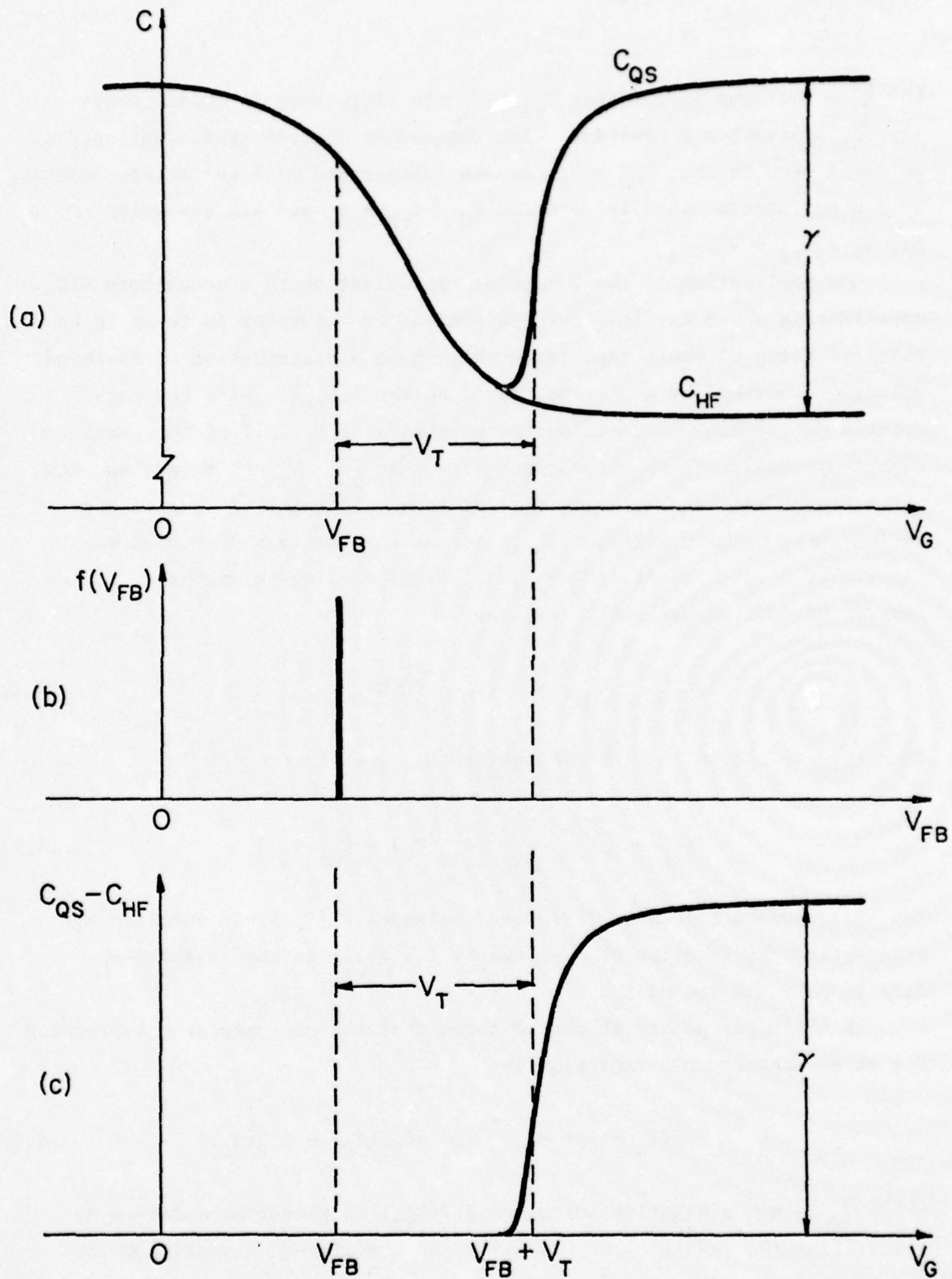

Fig. 22. (a) Typical quasi-static and high-frequency C-V curves for a uniform MOS capacitor with negligible interface states. (b) Distribution function of flatband voltages. (c) $C_{QS} - C_{HF}$, to be approximated by a step function in the analysis.

For gate voltages larger than $V_{FB} + V_T$ the difference in capacitances rapidly approaches a constant value denoted by γ. The approximation that we shall make is that $C_{QS} - C_{HF}$ can be represented with sufficient accuracy by a step function that is zero for $V_G < V_{FB} + V_T$ and has the value γ for $V_G > V_{FB} + V_T$.

The application of the foregoing approximation to a nonuniform MIS capacitor is shown in Fig. 23. The nonuniform capacitor is taken to be a parallel array of small capacitors which have a distribution of flatband voltages described by a distribution function $f(V_{FB})$. With the gate voltage of the nonuniform capacitor at the value V_G, all of the small capacitors having flatband voltages less than $V_G - V_T$ are turned on, and those having flatband voltages greater than this value are turned off. An increment of gate voltage dV_G increases the fraction of turned-on capacitors by the amount $f(V_G - V_T)dV_G$, thus causing an increment in the capacitance-difference curve given by

$$d(C_{QS} - C_{HF}) = \gamma f(V_G - V_T)dV_G \tag{4.1}$$

From this we obtain for the p-substrate MIS capacitor:

$$f(V_G - V_T) = \frac{1}{\gamma}\frac{d}{dV_G}[C_{QS}(V_G) - C_{HF}(V_G)] \tag{4.2}$$

The distribution function of flatband voltages, $f(V_{FB})$, is obtained by translating the function of V_G given by Eq. (4.2) in the negative-V_G direction by the amount V_T.

In a similar manner it can be shown that the corresponding expression for an n-substrate MIS capacitor is

$$f(V_G - V_T) = -\frac{1}{\gamma}\frac{d}{dV_G}[C_{QS}(V_G) - C_{HF}(V_G)] \tag{4.3}$$

where V_T is now a negative voltage and $f(V_{FB})$ is therefore obtained by translating the result of Eq. (4.3) in the positive-V_G direction by the amount $|V_T|$.

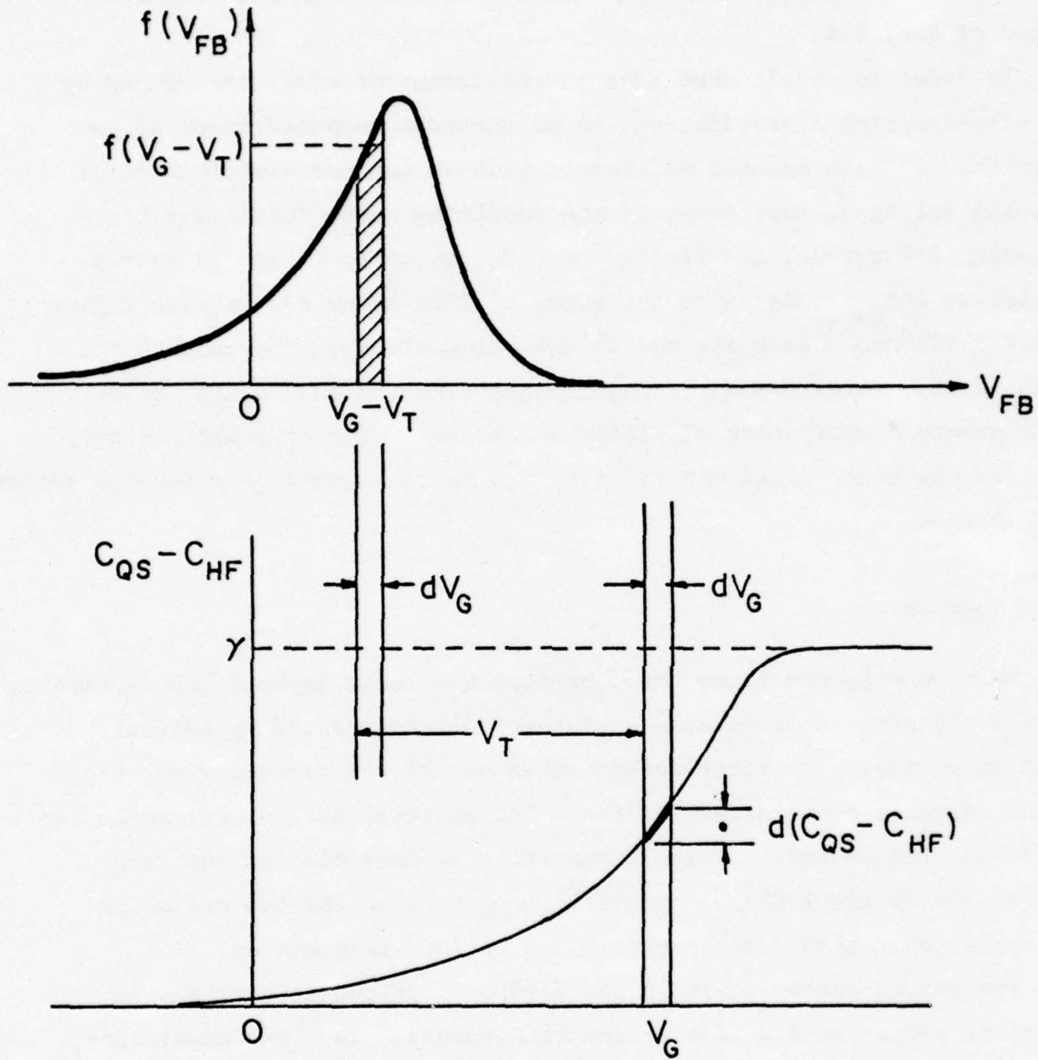

Fig. 23. Illustrating the connection betwen the distribution function of flatband voltages, $f(V_{FB})$, and the resulting capacitance-difference curve.

The foregoing relationships were the ones used in the comparison method of Sec. 4.4.

In order to obtain some idea of the amount of error introduced by the step-function approximation, we conducted a computer study of two examples. In each example we started with an assumed distribution of flatband voltages, then computed the resulting quasi-static and high-frequency C-V curves, and finally used Eq. (4.2) to obtain an approximation to $f(V_{FB})$. An oxide thickness of 2500 Å and a substrate doping of 3.3×10^{15} cm^{-3} were assumed in the calculations. The results are shown in Fig. 24(a) for a rectangular distribution and in Fig. 24(b) for a smooth distribution of flatband voltages. The agreement is only fair for the sharp-edged distribution but is reasonably good for the smooth distribution.

4.6. Summary

We have proposed three new capacitance-voltage methods for distinguishing between the effects of interface states and those caused by lateral nonuniformities. The first method makes use of the frequency dependence of the response of interface states. One measures the C-V curves at two different frequencies, as widely separated as possible, in the range between 100 Hz and 1 GHz. Any discrepancy between the two curves in the depletion regime must be attributed to interface states.

The second method utilizes the freeze-in of charge carriers in interface states at liquid-nitrogen temperature. The low-temperature, high-frequency C-V curve is measured while sweeping the gate voltage from accumulation into deep depletion at a reasonably fast rate, say 1 V/sec. If the lower portion of this curve is not parallel to the ideal curve at the same temperature, the sample has appreciable lateral nonuniformities. If the lower portion of the curve is parallel to the ideal curve at the same temperature, then all of the room-temperature C-V stretch-out is due to interface states.

The third method makes use of the fact that although the stretch-out of either a quasi-static or a high-frequency C-V curve caused by interface

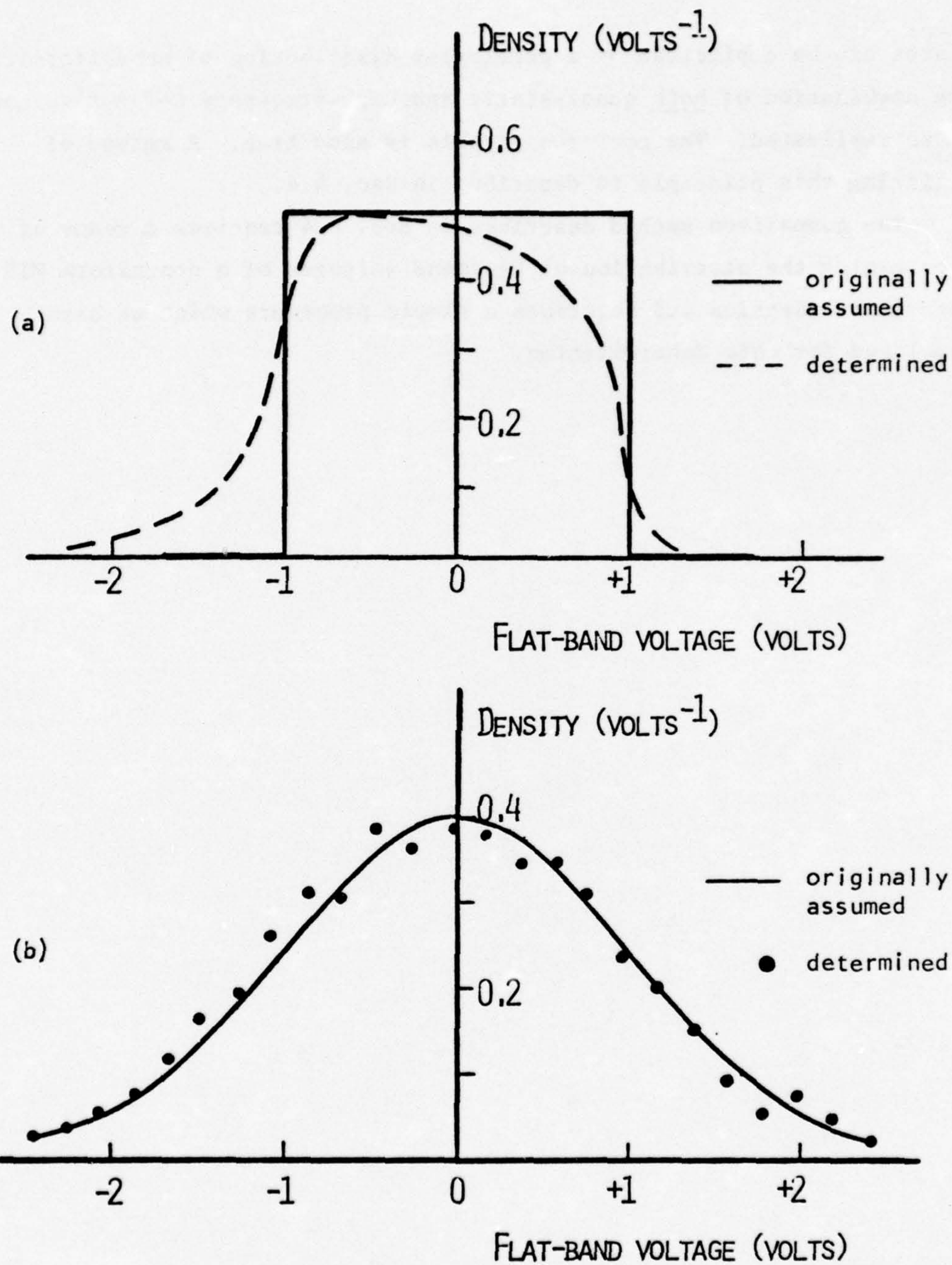

Fig. 24. Error analysis of the proposed technique [Eqs. (4.2) and (4.3)] for the determination of flat-band voltage distribution.

states can be duplicated by a particular distribution of nonuniformities, the combination of both quasi-static and high-frequency C-V curves can not be so duplicated. The converse of this is also true. A method of utilizing this principle is described in Sec. 4.4.

The comparison method described in Sec. 4.4 requires a means of determining the distribution of flatband voltages of a nonuniform MIS capacitor. Section 4.5 describes a simple procedure which we have developed for this determination.

REFERENCES

1. C. W. Perkins, K. G. Aubuchon, and H. G. Dill, IEEE Trans. Nucl. Sci. NS-15, 176 (1968).
2. R. P. Donovan, M. Simons, and L. K. Monteith, IEEE Trans. Nucl. Sci. NS-16, 203 (1969).
3. H. L. Hughes, 9th Annual Proceedings, Reliability Physics, Las Vegas, 1971, IEEE Catalog No. 71-C-9-Phy (IEEE, New York, 1971).
4. R. P. Donovan and M. Simons, J. Appl. Phys. 43, 2897 (1972).
5. H. L. Hughes, R. D. Baxter, and B. Phillips, IEEE Trans. Nucl. Sci. NS-19, 256 (1972).
6. K. H. Zaininger, Appl. Phys. Lett. 8, 140 (1966).
7. R. Williams, Phys. Rev. 140, A569 (1965).
8. A. M. Goodman, Phys. Rev. 164, 1145 (1967).
9. R. J. Powell and G. F. Derbenwick, IEEE Trans. Nucl. Sci. NS-18, 99 (1971).
10. A. S. Grove, Physics and Technology of Semiconductor Devices (Wiley, New York, 1967), Chaps. 9 and 12.
11. S. M. Sze, Physics of Semiconductor Devices (Wiley, New York, 1969), Chap. 9.
12. N. M. Johnson, W. C. Johnson, and M. A. Lampert, "Electron Trapping in Ion-Implanted Silicon Dioxide Films on Silicon," Technical Report No. 1, Contract N00014-67-A-0151-0035, January 1974.
13. N. M. Johnson, W. C. Johnson, and M. A. Lampert, "Electron Trapping in Aluminum-Implanted Silicon Dioxide Films on Silicon," J. Appl. Phys. 46, 1216 (1975).
14. C. N. Berglund and R. J. Powell, J. Appl. Phys. 42, 573 (1971).
15. R. Castagne and A. Vapaille, C. R. Acad. Sci. (Paris) B270, 1347 (1970); Electron. Lett. 6, 691 (1970).
16. M. A. Lampert and P. Mark, Current Injection in Solids, (Academic Press, New York, 1970).
17. T. E. Everhart and P. E. Hoff, J. Appl. Phys. 42, 5837 (1971).
18. C-T Shih, "A Study of the Effects of Low-Energy Electron Irradiation on MOS Capacitors," Ph.D. Dissertation, Princeton University, June 1975.
19. N. F. Mott and R. W. Gurney, Electronic Processes in Ionic Crystals, (Dover Publications, New York, 1964).
20. C. C. Chang, "Study of Lateral Nonuniformities and Interface States in MIS Structures," Ph.D. Dissertation, Princeton University, Feb. 1976.
21. R. Castagne and A. Vapaille, Electron. Lett. 6, 691 (1970).
22. L. M. Terman, Solid-State Electron. 5, 285 (1962).
23. P. V. Gray and D. M. Brown, Appl. Phys. Lett. 8, 31 (1966).
24. C. N. Berglund, IEEE Trans. Electron Devices, ED13, 701 (1966).

25. M. Kuhn, Solid-State Electron. 13, 873 (1970).

26. R. Castagne and A. Vapaille, Surf. Sci. 28, 157 (1971).

27. E. H. Nicollian and A. Goetzberger, Bell Syst. Tech. J. XLVI, 1055 (1967).

28. J. R. Brews and A. D. Lopez, Solid-State Electron. 16, 1267 (1973).

29. J. R. Brews, J. Appl. Phys. 43, 3451 (1972).

30. N. Gordon, "Investigation of the Properties of MIS and MNOS Structures," Ph.D. Dissertation, Princeton University (1974).

31. A. Goetzberger and J. C. Irvin, IEEE Trans. Electron Dev. ED-15, 1009 (1968).

32. S. Sze, Physics of Semiconductor Devices, (Wiley, New York, 1969), Ch. 10. A convenient chart giving values of V_T for various substrate dopings and SiO_2 thicknesses is given on p. 521 of this reference.

DISTRIBUTION LIST

Director
Defense Communications Agency
Washington, D.C. 20305
Attn: Code B210 Wpn. Sys. Anal. Div.
Attn: Code 540, Mr. Joseph A. Krcek

Defense Documentation Center
Cameron Station
Alexandria, Virginia 22314
Attn: TC (12 copies)

Commander
Defense Electronic Supply Center
1507 Wilmington Pike
Dayton, Ohio 45401
Attn: ECS

Director
Defense Intelligence Agency
Washington, D.C. 20301
Attn: DI-7B, Duane Voeller

Director
Defense Nuclear Agency
Washington, D.C. 20305
Attn: DDST, Mr. Peter H. Haas
Attn: RAEV (16 copies)
Attn: STVL (VLWS)
Attn: APTL (Technical Library) (2 copies)
Attn: APSI (Archives)
Attn: R. A. Poll

Director of Defense Research & Engineering
Washington, D.C. 20301
Attn: L. Weisberg
Attn: OAD(SW) Mr. G. R. Barse

Commander
Field Command
Defense Nuclear Agency
Kirtland AFB, New Mexico 87115
Attn: Technical Library FCWS-SC

Chairman
Joint Chiefs of Staff
Washington, D.C. 20301
Attn: J-6 CSD-1

Defense Advanced Research Projects Agency
1400 Wilson Boulevard
Arlgington, Virginia 22209
Attn: G. H. Heilmeier
Attn: STO Lt. Col. R. P. Sullivan

Director
Joint Strategic Target Planning Staff
Offutt AFB
Omaha, Nebraska 68113
   Attn: JLTW

Chief
Livermore Division, Field Command DNA
Lawrence Livermore Laboratory
P.O. Box 808
Livermore, California 94550
   Attn: L-395

Director
National Security Agency
Ft. George G. Meade, Maryland 20755
   Attn: D. O. Van Gunten - R-425

Director
Weapons Systems Evaluation Group, ODDR&E
Office, Secretary of Defense
400 Army-Navy Drive
Washington, D.C. 20305
   Attn: Capt. Donald E. McCoy, USN

Director
Advanced Ballistic Missile Defense Agency
Commonwealth Bldg.
1320 Wilson Blvd.
Arlington, Virginia 22209
   Attn: CRDABM-EO, Dr. R. S. Ruffine

Commandant
Army Air Defense School
Fort Bliss, Texas 79916
   Attn: ATSAD-DL-P

Commanding Officer
Army Material Systems Analysis Agency
U.S. Army Aberdeen Research & Development Center
Aberdeen Proving Round, Maryland 21005
   Attn: Ronald A. Marking

Commanding Officer
Army Mobility Equipment R & D Center
Fort Belvoir, Virginia 22060
   Attn: AMSEL-NV-SD, J. H. Carter

Commanding Officer
Atmospheric Sciences Laboratory, USAECOM
White Sands Missile Range, New Mexico 88002
Attn: AMSEL-BL-DD

Director
Ballistic Research Laboratories
Aberdeen Proving Ground, Maryland 21010
Attn: AMXRD-BNL, Technical Library
Attn: AMXRD-BVL, J. H. McNeilly
Attn: AMXRD-BVL, J. W. Kinch
Attn: AMXRD-BRD, Mr. Harrison

Chief of Research & Development
Department of the Army
Washington, D.C. 20310
Attn: NCB Division
Attn: DARD-MD, Ltc. Sloan

Commanding Officer
Frankford Arsenal
Bridge and Tacony Streets
Philadelphia, Pennsylvania 19137
Attn: N5000 Marvin Elnick
Attn: U1000 Bernard Schein

Department of the Army
Harry Diamond Laboratories
Washington, D.C. 20438
Attn: Technical Library
Attn: AMXDO-RBF, Dr. Edward E. Conrad, Chief, Lab200
Attn: AMXDO-RBG, Mr. Robert E. McCoskey, Chief, BR-280
Attn: AMXDO-NP, Mr. Francis Wimenitz, Chief, NWEPU
Attn: AMXDO-EM, J. R. Miletta

Commanding Officer
Picatinny Arsenal
Dover, New Jersey 07801
Attn: SMUPA-TY, Philip Zirkind
Attn: SMUPA-TC 3, Mr. R. Kesselman
Attn: SMUPA-VC5, Mrs. Ruth Nicolaides
Attn: SMUPA ND-N-E

Commanding General
Safeguard System Command
P.O. Box 1500
Huntsville, Alabama 35807
Attn: SSC-DH, Col. Robert A. Purple

Director
U.S. Army Advanced Ballistic Missile Defense Agency
Huntsville Office
P.O. Box 1500
Huntsville, Alabama 35807
Attn: RDMH-O
Attn: RDMH-X

U.S. Army Combat Developments Command
Nuclear Agency
Fort Bliss, Texas 79916
Attn: CDCNA-E

Chief
U.S. Army Combat Developments Command
Communications-Electronics Agency
Fort Monmouth, New Jersey 07703
Attn: Chief, M/E Div.

Commanding Officer
U.S. Army Combat Developments Command
Armor Agency
Fort Knox, Kentucky 40121

Commanding Officer
U.S. Army Combat Developments Command
Institute of Land Combat
2461 Eisenhower Avenue
Alexandria, Virginia 22314
Attn: CDILC-MTCS

Commanding Officer
U.S. Army Combat Developments Command
Artillery Agency
Fort Sill, Oklahoma 73503
Attn: CDCFA-ME, Maj. Ply.

Commanding General
U.S. Army Computer Systems Command
Fort Belvoir, Virginia 22060
Attn: CSCS-TME-E, Mr. E.T. Parker
Attn: CSCS-TME-C

Commanding General
U.S. Army Electronics Command
Fort Monmouth, New Jersey 07703
Attn: AMSEL-GG-TD, Miss Sarah Omanson
Attn: AMSEL-TN-N, Evans Bldg. 45, Dr. E. Both
Attn: AMSEL-TL-ND, Dr. E. T. Hunter

Commanding Officer
U.S. Army Materials & Mechanics Research Center
Watertown, Massachusetts 02172
Attn: AMXMR-XH, Mr. John Dignam

Commanding General
U.S. Army Material Command
Washington, D.C. 20315
Attn: AMCRD-MA, Rm. 2707, Mr. C.F. McGregor
Attn: AMCMS-IS, Mr. Aldric Saucier - Staff Adm.
Attn: AMCRD-WN, Mr. John J. F. Corrigan

Commanding General
U.S. Army Missile Command
Redstone Arsenal
Huntsville, Alabama 35809
Attn: AMSMI-RBLD, Chief, Document Section
Attn: AMSMI-RGP, Mr. Kenneth W. Plunkett
Attn: AMSMI-RGG, Mr. J. Holeman
Attn: AMCPM-MDE, Maj. Stanley

Commanding General
U.S. Army Munitions Command
Picatinny Arsenal
Dover, New Jersey 07801
Attn: CE/NED, Bldg. 65, Amina Nordio
Attn: NDB 300, Bldg. 95, Arthur Nichols

Commanding General
U.S. Army Security Agency
Arlington Hall Station
Arlington, Virginia 22212
Attn: IARD-EL

Commanding General
U.S. Army Tank Automotive Command
Warren, Michigan 48089
Atn: LTC. C. F. Dupke, AMCPM-MBT-SEW

Commanding General
U.S. Army Test and Evaluation Command
Aberdeen Proving Ground, Maryland 21005
Attn: AMSTE-NB, R. R. Galasso
Attn: AMSTE-EL, R. I. Kolchin

Commanding General
White Sands Missile Range, New Mexico 88002
Attn: STEWS-TE-NI, R. Q. Dysart
Attn: TE-N, (Nuc. Wpns. Eff. Lab.) Mr. Marvin P. Squires

Commander
Naval Air Systems Command
Headquarters
Washington, D.C. 20360
Attn: AIR-310, Research Administrator

Commanding Officer
Naval Ammunition Depot
Crane, Indiana 47522
Attn: Code 7024, Mr. James L. Ramsey

Commander
Naval Electronic Systems Command
Headquarters
Washington, D.C. 20360
Attn: PME, 117-21
Attn: ELEX 0518

Commander
Naval Electronics Laboratory Center
San Diego, California 92152
Attn: Code 3100, Mr. E. E. McCown
Attn: Code 3200, Mr. H. P. Wong

Commander
Naval Ordnance Laboratory
Silver Spring, Maryland 20910
Attn: 1-315, Technical Library (2 copies)
Attn: Code 121, Navy Nuclear Programs Office
Attn: Code 431, Norman Taslitt

Commander
Naval Ordnance Systems Command
Headquarters
Washington, D.C. 20360
Attn: ORD-034C, Mr. S. Barram
Attn: ORD-0523, Mr. R. Lane

Superintendent
Naval Postgraduate School
Monterey, California 93940
Attn: Library (Code 2124)

Director
Naval Research Laboratory
Washington, D.C. 20390
Attn: Code 2027, Technical Library (4 copies)
Attn: Code 5216, Mr. H. L. Hughes
Attn: Code 6460, Dr. Dean Mitchell
Attn: Code 5210, Dr. Davey
Attn: Code 7001, Mr. J. D. Brown
Attn: Code 4004, Dr. E. L. Brancato

Commander
Naval Ship Engineering Center
Center Building
Prince Georges Center
Hyattsville, Maryland 20782
  Attn: Edward L. Berkowitz

Command Officer
Naval Weapons Evaluation Facility
Kirtland Air Force Base
Albuquerque, New Mexico 87117
  Attn: Code WE, Mr. Stanley

Command Officer
Naval Weapons Station
Concord, California 94520
  Attn: Qual. Eval. Lab., Code 33120, Dr. Robert Wagner

Director
Strategic Systems Project Office
Department of the Navy
Washington, D.C. 20390
  Attn: SP-230, Mr. David Gold
  Attn: SP-273, Mr. Phil Spector

Argonne National Laboratory
9700 South Cass Avenue
Argonne, Illinois 60439
  Attn: Document Control for E.N. Pettitt

Assistant General Manager for Military Application
U.S. Atomic Energy Commission
Washington, D.C. 20545
  Attn: CDR, Wayne L. Beech/LTC. Donald C. Little

Bendix Corporation, The
P.O. Box 1159
Kansas City, Missouri 64141
Attn: D.D. Peterson, D863-FB39
Attn: Richard A. Mehnert

Los Alamos Scientific Laboratory
P.O. Box 1663
Los Alamos, New Mexico 87544
Attn: Terry R. Gibbs, GMX-7

Sandia Laboratories
P.O. Box 5800
Albuquerque, New Mexico 87115
Attn: Document Control for Technical Library
Attn: Document Cotnrol for Org. 1930, J.A. Houd
Attn: Document Control for R. L. Ewing, 1532
Attn: Document Control for Org. 1933, F. N. Coppage
Attn: Document Control for Org. 1935, J. B. Gover
Attn: Document Control for C. N. Vittitoe

Sandia Laboratories
Livermore Laboratory
P.O. Box 969
Livermore, California 94550
Attn: Document Control for John L. Wirth
Attn: Document Control for Kenneth A. Mitchell
Attn: Document Control for Kenneth W. Dolan
Attn: Document Control for Theodore A. Dellin

University of California
Lawrence Livermore Laboratory
Technical Information Division
P.O. Box 808
Livermore, California 94550
Attn: Technical Information Department L-3
Attn: L-21, Dr. H. P. Smith Jr.
Attn: L-31, William J. Hogan
Attn: Hans Kruger L-24
Attn: Dr. David Oakley L-24
Attn: L. L. Cleland L-156

Central Intelligence Agency
Washington, D.C. 20505
Attn: Ralph Rostron
Attn: Alice Padgett

Department of Commerce
National Bureau of Standards
Washington, D.C. 20234
Attn: Applied Rad. Div., Dr. Robert C. Placious
Attn: Judson C. French, Chief, Electron Dev. Sec.

National Aeronautics and Space Administration
Lewis Research Center
21000 Brookpark Road
Cleveland, Ohio 44135
Attn: Library (NO R/D)

National Aeronautics and Space Administration
Washington, D.C. 20546
Attn: Code REE, Guidance, Control & Information Sys.

Aeroject Electro-Systems Co. Div.
Aeroject-General Corporation
P.O. Box 296
Azusa, California 91702
Attn: Thomas D. Hanscome, 6181/170
Attn: Roy Y. Kakuda, B-194/D-6121

Aerospace Corp.
P.O. Box 5866
San Bernardino, California 92408
Attn: Technical Library
Attn: J. J. Butts
Attn: William W. Willis
Attn: WPNS, Eff. Dept., Dr Julian Reinheimer

Aerospace Corporation
P.O. Box 95085
Los Angeles, California 90045
Attn: Francis Hai
Attn: Mr. I. M Garfunkel - Bldg 115 - Rm 2065
Attn: L. W. Aukerman - Bldg. 120 - Rm 2841
Attn: Library Acquisition Group
Attn: Dr. V. Josephson

American Nucleonics Corporation
6036 Variel Avenue
Woodland Hills, California 91364
Attn: Security Officer for G. L. Brown

Analog Technology Corporation
3410 East Foothill Boulevard
Pasadena, California 91107
Attn: John Joseph Baum

Applied Physics Laboratory
Johns Hopkins University
8621 Georgia Avenue
Silver Spring, Maryland 20910
Attn: Mr. Peter E. Partridge

Art Research Corporation
1100 Glendon Avenue
Los Angeles, California 90024
Attn: Arthur Sanders

AVCO
Government Products Group
201 Lowell Street
Wilmington, Massachusetts 01887
Attn: Research Library, A220, Room 2201

AVCO Corporation
Electronics Division
2630 Glendale-Milford Road
Cincinnati, Ohio 45241
Attn: AVED-048275, Lois Hammond

Battelle Memorial Institute
505 King Avenue
Columbus, Ohio 43201
Attn: Richard K. Thatcher

Beech Aircraft Corporation
9709 East Central Avenue
Wichita, Kansas 67201
Attn: Edward L. Radell

Bell Aerospace Company
Division of Textron, Inc.
P.O. Box 1
Buffalo, New York 14240
Attn: Martin A. Henry, Mail Stop F-11

Bell Telephone Laboratories, Inc.
2120 Pinecroft Road
Greensboro, North Carolina 27407
Attn: James P. Sweeney
Attn: Charles E. Boyle

Bell Telephone Laboratories, Inc.
Mountain Avenue
Murray Hill, New Jersey 07971
Attn: Mr. Donald K. Wilson
Attn: R. D. Taft, Room 2B-190
Attn: E. C. Snyder, Room WH-2B-190
Attn: H.A. Jarrell, Room WH-2B-153
Attn: Mr. William E. Brady

Bendix Corporation, The
Research Laboratories Division
Bendix Center
Southfield, Michigan 48075
Attn: Mgr., Program Devel., Mr. Donald J. Niehaus

Bendix Corporation, The
Aerospace Systems Division
3300 Plymouth Road
Ann Arbor, Michigan 48107
Attn: Mr. Ronald H. Pizarek

Bendix Corporation, The
Navigation and Control Division
Teterboro, New Jersey 07608
Attn: E. E. Lademann
Attn: T. Lavin, Dept. 7111

Boeing Company, The
P.O. Box 3707
Seattle, Washington 98124
Attn: Dr. David L. Dye, M.S. 89-76
Attn: A. R. Lowrey, M.S. 2R-00
Attn: H. W. Wicklein, M.S. 1F-51
Attn: R. S. Caldwell, M.S. 2R-00
Attn: R. Seiler, M.S. 2R-00

Booz-Allen Applied Research, Inc.
Room 600
911 Walnut Street
Kansas City, Missouri 64106
Attn: Frederick Newton

Braddock, Dunn & McDonald, Inc.
P.O. Box 8441, Station C
Albuquerque, New Mexico 87108
Attn: Robert B. Buchanan

Braddock, Dunn & McDonald, Inc.
8027 Leesburg Pike
McLean, Virginia 22101
Attn: Mr. Lin R. Albright
Attn: Dr. J. V. Braddock
Attn: A. Lavagnino

Brown Engineering Company, Inc.
Research Park
Huntsville, Alabama 35807
Attn: David Lambert, M.S. 126

Burroughs Corporation
Defense, Space & Special Systems Group
Central Ave. & Route 202
Paoli, Pennsylvania 19301
Attn: R. L. Davis

California Institute of Technology
Jet Propulsion Laboratory
4800 Oak Grove Drive
Pasadena, California 91103
Attn: Paul Pietrokowsky

Chrysler Corporation
Defense Division
P.O. Box 757
Detroit, Michigan 48231
Attn: R. F. Gentile - CIMS #435-01-21

Collins Radio Company
5225 C Avenue, N.E.
Cedar Rapids, Iowa 52406
Attn: W.C. Fackler, Structural Systems Group Head

Cornell Aeronautical Laboratory, Inc.
P.O. Box 235
Buffalo, New York 14221
Attn: R. H. Dickhaut, Bldg. 10, Rm. 341

Dikewood Corporation, The
1009 Bradbury Drive, S.E.
University Research Park
Albuquerque, New Mexico 87106
Attn: L. Wayne Davis, Asst. Vice Pres.

Effects Technology, Inc.
5383 Holister Avenue
Santa Barbara, California 93105
Attn: Edward John Steele

EG&G, Inc.
P.O. Box 227
Bedford, Massachusetts 01730
Attn: Paul McLellan

EG&G, Inc.
San Ramon Operations
P.O. Box 204
San Ramon, California 94583
Attn: Burnell G. West

Electronic Communications, Inc., Subsidiary of NCR
P.O. Box 12248
Saint Petersburg, Florida 33733
Attn: Dept. 623, J. T. Daniel

Energy Conversion Devices, Inc.
1675 West Maple Road
Troy, Michigan 48084
Attn: Mr. Lionel Robbins

Fairchild
Space & Defensive Systems Division
300 Robins Lane
Syosset, New York 11791
Attn: W. Wylde

Fairchild Camera & Instrument Corporation
Research & Development Division
4001 Miranda Avenue
Palo Alto, California 94304
Attn: 30-204, Mr. David K. Myers, Radiation Conslt.

Florida, University of
Gainesville, Florida 32603
Attn: Prof. J. A. Samuel, M.E. Dept.

Garrett Corporation, The
Airesearch Manufacturing Company Division
9851 Sepulveda Blvd.
Los Angeles, California 90009
Attn: Robt. Weir, Dept. 93-9

General Dynamics Corp.
Convair Aerospace Division
San Diego Operations
P.O. Box 1950
San Diego, California 92112
Attn: Library, Mr. D. H. McCoy

General Electric Company
Tempo-Center for Advanced Studies
816 State Street (P.O. Drawer QO)
Santa Barbara, California 93102
Attn: DASIAC

General Electric Company
Aerospace Electronics Department
French Road
Utica, New York 13502
Attn: W. J. Patterson, Drop 233

General Electric Company
Avionics Controls Department
P.O. Box 5000
Binghamton, New York 13907
Attn: B. H. Showalter(Mail Drop 16)

General Electric Company
P.O. Box 1122
Syracuse, New York 13201
  Attn: HMES, Bldg. 1, Rm. 4, J. R. Greenbaum
  Attn: CSP 6-7, L. H. Dee

General Electric Company
Re-Entry & Environmental Systems Division
P.O. Box 7722
Philadelphia, Pennsylvania 19101
  Attn: William L. Chadsey
  Attn: Robert V. Benedict

General Electric Company
Space Division
Valley Forge Space Center
P.O. Box 8555
Philadelphia, Pennsylvania 19101
  Attn: Radiation Eff., Lab. Mr. John L. Andrews

General Electric Company
Ordnance Systems
100 Plastics Avenue
Pittsfield, Massachusetts 01201
  Attn: David Corman (Mail No. 2276)

General Electric Company
Aircraft Engine Group
Evendale Plant
Cincinnati, Ohio 45215
  Attn: John A. Ellerhorst, E 2

General Motors Corporation
Delco Electronics Division
7929 South Howell Avenue
Milwaukee, Wisconsin 53201
  Attn: Technical Library 2A07 (E. T. Krueger)

General Physics Corporation
Banneker Building
Colukbia, Maryland 21043
  Attn: Robert W. Deutsch

General Research Corporation
1501 Wilson Blvd.
Arlington, Virginia 22209
  Attn: Dr. Robert M. Chmieleski

General Research Corporation
P.O. Box 3587
Santa Barbara, California 93105
  Attn: Tech. Info. Office for Dr. John Ise, Jr.

Grumman Aerospace Corporation
South Oyster Bay Road
Bethpage, New York 11714
  Attn: Dept. 535, PT 35, J. Rogers

Gulf Oil Corporation
P.O. Box 1111
San Diego, California 92112
  Attn: Victor A. J. Van Lint, GRT
  Attn: R. Mertz, GRT
  Attn: R. Overmyer, GRT
  Attn: Leo D. Cotter, GRT
  Attn: J. A. Naber, GRT
  Attn: Roland E. Leadon, GRT
  Attn: T. M. Flanigan, GRT

Hamilton Standard
Division of United Aircraft Corporation
Bradley International Airport
Windsor Locks, Connecticut 06096
  Attn: Raymond G. Giguere

Honeywell, Inc.
Aerospace Division
13350 U.S. Highway 19
St. Petersburg, Florida 33733
  Attn: M.S. 724-5, Mr. James D. Allen, Adv. Dev.
  Attn: R. C. Schrader, Sr. Prin. Eng., M.S. 725-5
  Attn: Harrison H. Noble Staff Engineer, M.S. 725-5A
  Attn: William England
  Attn: M.S. 725-5 Stacey H. Graff

Honeywell, Inc.
Radiation Center
2 Forbes Road
Lexington, Massachusetts 02173
  Attn: Technical Library

Honeywell, Inc.
Aeronautical Division
2600 Ridgway Road
Minneapolis, Minnesota 55413
  Attn: Ronald R. Johnson A1391

Hughes Aircraft Company
Centinela Avenue and Teale Street
Culver City, California 90230
  Attn: M.S. 6/E110, B. W. Campbell
  Attn: R&D Division, William A. McDowell
  Attn: R&D Division, Ross M. Orndorff
  Attn: R&D Division, Dr. Dan Binder (M.S. D147)

IIT Research Institute
Electromagnetic Compatability Analysis Center
North Severn
Annapolis, Maryland 21402
  Attn: ACOAT

Institute for Defense Analyses
400 Army-Navy Drive
Arlington, Virginia 22202
  Attn: Technical Information Office

International Business Machines Corporation
Route 100
Owego, New York 13827
  Attn: Mr. Daniel C. Sullivan, Dept. M40, 102-1

International Telephone and Telegraph Corporation
500 Washington Avenue
Nutley, New Jersey 07110
  Attn: Defense-Space Group, SMTS, Frank Johnson
  Attn: Alexander L. Richardson

Isotopes, Inc.
50 Van Buren Place
Westwood, New Jersey 07675
  Attn: Dr. Peter Alexander

Kaman Sciences Corporation
Kaman Nuclear Division
1700 Garden of the Gods Road
Colorado Springs, Colorado 80907
  Attn: Dr. Albert P. Bridges
  Attn: N-Gamma Lab., Dr. Don Bryce
  Attn: Dr. Frank H. Shelton

Litton Systems, Inc.
Mellonics Systems Development Division
1001 West Maude Avenue
Sunnyvale, California 94086
  Attn: Sam Sternbach, Data Systems Division

Litton Systems, Inc.
Electron Tube Division
1035 Westminster Drive
Williamsport, Pennsylvania 17701
Attn: Frank J. McCarthy

Lockheed Missiles and Space Company
3251 Hanover Street
Palo Alto, California 94304
Attn: Dr. Clarence F. Kooi, Dept. 52-11, Bldg. 204
Attn: Dept. 52-11/203, Mr. Edwin A. Smith

Lockheed Missiles and Space Company
Division of Lockheed Aircraft Corporation
P.O. Box 504
Sunnyvale, California 94088
Attn: H. Schneemann, Org. 81-62
Attn: Tech. Info. Ctr., Dr. W.A. Kozumplik, Bldg. 201

LTV Aerospace Corporation
Vought Missiles & Space Company
Michigan Division
P.O. Box 909
Warren, Michigan 48090
Attn: Mr. T. M. Rozelle

LTV Electrosystems, Inc.
Major Field
P.O. Box 1056
Greenville, Texas 75401
Attn: Library

M.I.T. Lincoln Laboratory
P.O. Box 63
244 Wood Street
Lexington, Massachusetts 02173
Attn: Alan G. Stanley

Martin Marietta Corporation
Orlando Division
P.O. Box 5837
Orlando, Florida 32805
Attn: Mr. William W. Mras, MP-413

Massachusetts Institute of Technology
77 Massachusetts Avenue, Room 24-120
Cambridge, Massachusetts 02139
Attn: Mr. Kenneth Fertig, M.S. 87
Attn: Mr. Richard G. Haltmaier

McDonnell Douglas Corporation
5301 Bolsa Avenue
Huntington Beach, California 92647
  Attn: N. L. Andrade, M.S. 17, BBDO Adv Elect/R&D

McDonnell Douglas Corporation
P.O. Box 516
St. Louis, Missouri 63166
  Attn: Dr. Tom Ender, Dept. 313, Bldg. 33

Minnesota, University of
2030 University Avenue, S.E.
Minneapolis, Minnesota 55414
  Attn: Dr. A. Van der Ziel, Elec. Eng. Dept.

Mission Research Corporation
812 Anacapa Street
Santa Barbara, California 93101
  Attn: W. A. Schlueter

Mitre Corporation, The
Route 62 and Middlesex Turnpike
P.O. Box 208
Bedford, Massachusetts 01730
  Attn: M.E. Fitzgerald
  Attn: Library

Motorola, Inc.
Government Electronics Division
8201 E. McDowell Road
Scottsdale, Arizona 85252
  Attn: Philip L. Clar

Motorola, Inc.
Semiconductor Products Division
5005 East McDowell Road
Phoenix, Arizona 85008
  Attn: Sr. Scientist, Mr. Clarence A. Lund, MD-A130
  Attn: Mgr , Mtrls. Tech., Mr. James R. Black, MD-B136

New Mexico, University of
Dept. of Campus Security
Carlisle Gymnasium
Albuquerque, New Mexico 87106
  Attn: Dr. W. W. Grannemann

North American Rockwell Corporation
Autonetics, Electronics Group
3370 Miraloma Avenue
Anaheim, California 92803
  Attn: G. Messenger
  Attn: J. Bell
  Attn: D. Bausch

North American Rockwell Corporation
Space Division
12214 South Lakewood Boulevard
Downey, California 90241
  Attn: Code FB 82, David Champaign

Columbus Division
North American Rockwell Corporation
4300 East Fifth Avenue
Columbus, Ohio 43216
  Attn: Engineering Data Services (J.F. Roberts)

Northrop Corporation
Northrop Corporate Laboratories
3401 West Broadway
Hawthorne, California 90250
  Attn: Mr. James P. Raymond
  Attn: Dir., Solid St. Elec., Dr. Orlie L. Curtis, Jr.

Northrop Corporation
Electronic Division
2301 West 120th Street
Hawthorne, California 90250
  Attn: Vincent R. DeMartino
  Attn: Boyce T. Ahlport

Palisades Institute for Research Services, Inc.
201 Varick Street
New York, New York 10014
  Attn: Records Supervisor

Philco-Ford Corporation
Aerospace & Defense Systems Operations
Aeronutronic Division
Ford & Jamboree Roads
Newport Beach, California 92663
  Attn: Peter H. Stadler
  Attn: Dr. L. H. Linder

Philco-Ford Corporation
Western Development Laboratories Division
3939 Fabian Way
Palo Alto, California 94303
  Attn: Library

Power Physics Corporation
Industrial Way West
P.O. Box 626
Eatontown, New Jersey 07724
Attn: Hyman Newman

R & D Associates
P.O. Box 3580
Santa Monica, California 90403
Attn: Mr. Richard R. Schaefer
Attn: Mr. S. C. Rogers

Radiation Incorporated
P.O. Box 37
Melbourne, Florida 32901
Attn: John H. Turner
Attn: Mr. Don Gibson

Raytheon Company
528 Boston Post Road
Sudbury, Massachusetts 01776
Attn: Harold L. Flescher
Attn: D. R. Jones

RCA Corporation
Government & Commercial Systems
Astro Electronics Division
P.O. Box 800
Princeton, New Jersey 08540
Attn: G. Brucker

RCA Corporation
David Sarnoff Research Center
201 Washington Road
West Windsor Township
Princeton, New Jersey 08540
Attn: Dr. K. H. Zaininger, Solid State Device Tech.

RCA Corporation
P.O. Box 591
Somerville, New Jersey 08876
Attn: Daniel Hampel, Adv. Comm. Lab.
Attn: Mr. Frank J. Feyder, Zone 77

Research Triangle Institute
P.O. Box 12194
Research Triange Park, North Carolina 27709
Attn: Eng. & Envir. Sci. Div., DR. Mayrant Simons, Jr.

Simulation Physics, Inc.
10 Railroad Avenue
Bedford, Massachusetts 01730
Attn: Mr. Roger G. Little

Singer-General Precision, Inc.
Kearfott Division
1150 McBride Avenue
Little Falls, New Jersey 07424
Attn: A. A. Witteles-RAD. Effects Supv. 3-5820

Sperry Rand Corporation
Sperry Rand Research Center
100 North Road
Sudbury, Massachusetts 01776
Attn: H.A.R. Wegener

Sperry Rand Corporation
Univac Division
Defense Systems Division
P.O. Box 3525 Mail Station 1931
St. Paul, Minnesota 55101
Attn: Mr. Dennis Amundson

Sperry Rand Corporation
Sperry Gyroscope Division
Great Neck, New York 11020
Attn: Dept. 4282 - Mr. P. Marraffino
Attn: Mr. C. Craig, 1P39

Stanford Research Institute
222 Ravenswood Avenue
Menlo Park, California 94025
Attn: Mr. Arthur Lee Whitson
Attn: Dr. Robert A. Armistead
Attn: James A. Baer, Sr. Res. Engineer, J1015
Attn: Mr. Philip Dulan

Stanford Research Institute
4810 Bradford Blvd., N.W.
Huntsville, Alabama 35805
Attn: Harold Carey

Sylvania Electronic Systems Group
Communications Systems Division
189 B Street
Needham, Massachusetts 02194
Attn: S/V Eng. Dept., J. A. Waldron

Systems, Science and Software, Inc.
P.O. Box 1620
La Jolla, California 92037
Attn: Dr. Ralph H. Stahl

Systron-Donner Corporation
200 San Miguel Road
Concord, California 94520
Attn: Harold D. Morris

Texas Instruments, Inc.
P.O. Box 5474
Dallas, Texas 75222
Attn: Walter Matzen
Attn: R&D Proj. Man., Dr. Donald J. Manus, M.S. 72
Attn: Radiation Effects Prog. Mgr. Mr. Gary F. Hanson

TRW Semiconductors
Division of TRW, Inc.
14520 Aviation Blvd.
Lawndale, California 90260
Attn: Gerald A. Schafer - Missile & Space Sub-Div.
Attn: Mr. Ronald N. Clarke, Member Technical Staff

TRW Systems Group
One Space Park
Redondo Beach, California 90278
Attn: Mr. A. Anderman R1/2036
Attn: Mr. R. Kingsland
Attn: Lillian Singletary R1/2154
Attn: Mr. D. Jurtner

United Aircraft Corporation
Norden Division
Helen Street
Norwalk, Connecticut 06851
Attn: Conrad Corda

Varian Associates
611 Hansen Way
Palo Alto, California 94304
Attn: D. C. Lawrence - Radiation Safety

Westinghouse Electric Corporation
Astronuclear Laboratory
P.O. Box 10864
Pittsburgh, Pennsylvania 15236
Attn: P. W. Dickson

Westinghouse Electric Corporation
Research and Development Center
1310 Beulah Road, Churchil Borough
Pittsburgh, Pennsylvania 15235
Attn: William E. Newell